Effect of time delay on the impedance control of a pressure-based, current-driven Electroacoustic Absorber

E de Bono, Manuel Collet, G Matten, Sami Karkar, H Lissek, M Ouisse, Kevin Billon, T Laurence, M Volery

Effect of time delay on the impedance control of a pressure-based, current-driven Electroacoustic Absorber.

E. De Bono[1], M. Collet[1], G. Matten[2], S. Karkar[1], H. Lissek[3], M. Ouisse[2], K. Billon[1], T. Laurence[3], and M. Volery[3]

[1]École Centrale de Lyon, LTDS laboratory, CNRS UMR5513, 36 avenue Guy de Collongue, 69134 Ecully Cedex, France

[2]Univ. Bourgogne Franche-Comté, FEMTO-ST Institute, Department of Applied Mechanics, CNRS/UFC/ENSMM/UTBM, 24 Chemin de l'Épitaphe, 25000 Besançon, France

[3]École polytechnique Fédérale de Lausanne, Laboratoire de traitement des signaux LTS2, Route Cantonale, 1015 Lausanne, Switzerland

August 22, 2022

Abstract

The pressure-based, current-driven impedance control technique known as "Electroacoustic Absorption" has offered new horizons for room modal equalization at low frequencies, steerable anomalous reflection, acoustic transmission attenuation and non-reciprocal wave propagation. Nevertheless, its level of performance is strongly limited by stability constraints. A primary source of instability is the loss of acoustical passivity due to time delay in the digital implementation of the controller. In this paper, the effect of time delay on the Electroacoustic Absorber stability is verified by correlating, both numerically and experimentally, the loss of acoustical passivity at high frequencies to the upsurge of instability in a one-dimensional closed cavity. Then, we show the effect of placing a porous layer in front of the Electroacoustic Absorber, allowing to counteract for the loss of acoustical passivity and enlarge the passivity margin. Finally, we provide an integral constraint on the absorption spectrum valid for the pressure-based, current-driven architecture of the Electroacoustic Absorber. It generalizes the integral constraint for purely passive absorbers to electro-active impedance controlled loudspeakers, and demonstrates the close interdependence between absorption bandwidth, passivity, and electrical source supply by a straightforward analytical expression.

1 Introduction

The Active Noise Cancellation (ANC) first experiment dates back likely to 1878 when Lord Rayleigh used two electromechanically synchronized tuning forks [1], [2]. The first patents of Active Noise Cancellation (by destructive interference) have been granted to H. Coanda [3], and few weeks later to Lueg [4],[2]. These noise control techniques have been defined as "feedforward" as they use a reference sensor placed upstream with respect to the actuator (in an acoustic waveguide). The "electronic sound absorber" of Olson and May [5] is the first analogical feedback system, as it did not need an upstream reference signal [2], [6], but just a pressure sensor close to the loudspeaker. Olson and May envisaged the possibility to use their "spot type noise reducer" behind an acoustical resistance, in order to create what Guicking [7] later called "an active equivalent of the $\lambda/4$ resonance absorber". Following the work of Guicking, the ANC was used to enhance the performance of a resistive layer in a flow duct at lower frequencies, by Galland et al [8]. The ambitious objective was to reproduce the Cremer's optimal impedance for the first duct mode [9], [10]. It used ANC such that the acoustic impedance of the passive layer would be equal to its flow resistivity at low frequencies, while purely passive behaviour would be assured at higher frequencies. A FX-LMS adaptive filter was adopted in order to achieve the hybrid behaviour. One advantage of this hybrid approach was the possibility to protect the control system from the hostile environment in flow ducts, in view of future applications into nacelle inlets of aircraft engines. Nevertheless, the complexities linked to the optimal impedance achievement, along with the difficulties arisen for broadband attenuation, limited this interesting approach.

The ANC progressed thanks to the digital systems, which allowed for adaptive filters to cope with the acoustic feedback and secondary path issues [2]. Feedback control evolved from local to global noise reduction, but with many difficulties mainly due to insufficient spatial modelling and neglect of the loudspeaker own mechanical dynamics into the desired control bandwidth [6]. Phase correction [11] and velocity compensation [12] were proposed by Clark and Lane to improve the stability margins.

But the collocation of pressure sensing and actuator, suggested another approach, different from the ANC, for active noise reduction: the impedance matching. The main advantage of the impedance matching techniques with respect to the ANC is the possibility to keep the *acoustical passive* character of the electroacoustic device, contrary to the ANC which is, by definition, an *acoustically active* technique, whose stability highly depends upon the external acoustic environment. An acoustically passive controlled device is instead inherently stable [13] and therefore insensitive to the external acoustic feedback, which is source of instability in the ANC. Therefore, *acoustical passivity* brings along higher robustness and integrability in complex environments, and allows potentially simpler and energetically cheaper control strategies. Nevertheless, the impedance control techniques are supposed to achieve the *acoustical passivity* in the target frequency bandwidth, but not necessarily outside of it, as we will show in the following.

The "relatively simple and straightforward" concept of impedance matching dates back to the work of Bobber [14] who used an electronic generator for "cancelling the internal acoustic reactance of the transducer" in a water-filled tube.

Guicking et al. [7] proposed an impedance matching in a one-dimensional (1D) waveguide by analogically implementing the two microphone method for retrieving the reflection coefficient to be minimized. The problem was then the application to a 3D field. The two microphones wave splitter idea was retrieved in [15], through a filtered-X LMS adaptive filter. The direct impedance control was also approached by processing simultaneously both the pressure and the loudspeaker velocity [16], the latter being measured with an accelerometer, and by using a reference signal from the primary source to avoid feedback instability.

The main problem of these direct impedance control strategies is the addition of intrusive sensors, such as accelerometers or frontal microphones, and the complexities related to the adaptive filters.
As the ANC improved thanks to the integration of the loudspeaker dynamics model into the control [12], also the impedance matching research found new interesting perspectives by querying how to exploit the actuator own electro-mechanical dynamics. In the realm of audio-engineering, De Boer [17] enounced a "motional feedback theory" to *self-sense* the loudspeaker velocity, based upon assumptions on the loudspeaker dynamics. Leo [18] developed a self-sensing technique to estimate both pressure and velocity by measuring speaker voltage and current, and damp cavity resonances through second order feedback compensators. Clearly, a sensorless technique requires a good electro-mechanical model of the loudspeaker. Leo's technique suffered from weak electro-mechanical coupling in the pressure estimation, and of inaccurate electrical impedance model despite the use a 5th order transfer function. Samejima [19], instead, proposed a differentiating circuit attached to a secondary coil (the "pick-up coil") to have a velocity estimation for a state-feedback impedance control. In the linear quadratic regulator (LQR) optimization used in [19], neither energy limits nor stability constraints could be taken into account, therefore resulting in feedback gains extremely high, and excessive sensitivity to model uncertainties. This prevented the experimental implementation of such technique. The double coil idea was developed also by Rivet et al. [20] who proposed a control strategy capable of attaining the target resistance at the resonance frequency, without the need of the loudspeaker model identification. In general, the use of a secondary coil allowed to get rid of any external sensor, rendering the impedance control system more compact. Nevertheless, the physical realizability in [19], and the restrained frequency bandwidth in [20], inhibited further investigations on this approach. Rather than controlling the acoustic impedance based upon acoustic variable sensing, acoustic impedance matching can also be achieved by modifying the electrical impedance of the loudspeaker itself, thanks to the electromechanical coupling. Lissek et al. [21] introduced an unified formulation of the "Electroacoustic Absorber" (EA) by demonstrating the equivalence between direct impedance control (based upon pressure and velocity sensing) and the shunting techniques. They highlighted how, on the one hand, the direct impedance control strongly depends upon the neutralization of the loudspeaker electrical impedance, therefore is limited by stability issues coming from wrong modelling of the electrical inductance. On the other hand, the electrical shunting equivalent, even though always stable, is often not easily realizable. The inherent stability of the shunting impedance controlled systems comes from their *acoustically passive* character. This is not necessarily the case for impedance control based upon synthesized correctors, because of both modelling inaccuracies and time delay in the digital implementation. Fleming [6] showed the effect of different electrical shunts, based upon a Hemholtz resonator analogy. He also designed an "active-shunt" control, in the sense that the shunt was substituted by a digital corrector, obtained with optimal control techniques (such as H_∞). The artificially synthesized electrical impedance achieved wider bandwidths of attenuation, and the physical modelling was substituted by experimentally identified "plant transfer functions", simplifying the design process on the one hand, but still being limited by system uncertainties on the other. The problem posed by the inductance model of the loudspeaker coil in the direct impedance control, was also encountered by Boulandet et al. [22], who identified it as a limitation due to a not-much-clarified "side effect of the Bode's sensitivity integral theorem". He tried to overcome this issue using lead-lag phase compensation, "ensuring that the electroacoustic resonator (ER) strictly remains a dissipative system over the whole frequency range of interest", but not beyond it, as long as the Bode's sensitivity integral constraint applies (it is the so-called "waterbed effect"). Finally, Rivet et al. [23] proposed an "hybrid sensor-/shunt-based impedance control" which is a mechanical-model-inversion-based control. It detected pressure with a microphone placed as close as possible to the loudspeaker to achieve quasi-collocation and drove the current

(thanks to a Howland current pump [24]) in order to equal out the own mechanical dynamics of the loudspeaker, and reproduce a desired acoustical impedance at the speaker interface. The Howland current pump on the one hand, and the use of a microphone on the other, allowed to restrict the model inversion to the mechanical dynamics only, getting rid of the electrical inductance modelling issues of the direct impedance control, and of the electrical shunting techniques. As the mechanical model uncertainties are much less critical than the electrical ones, it was possible to enlarge the frequency bandwidth of absorption. This control architecture proved great versatility and it has been adopted in various applications, such as room modal equalization [25], duct modes damping [26], broadband non-reciprocal acoustic propagation [27] and as a base for a non-linear control strategy [28]. A primary limitation of such "hybrid" sensor and model-inversion based impedance control is related to the loss of acoustical passivity caused by the time-delay in the digital implementation which causes high-frequency instabilities in a similar manner as the acoustic feedback in ANC. In this perspective, it is significant the work of Xia et al. [29], who have formalized a passivation method based upon an input-output transformation matrix, and have applied it to time-delayed systems.
The objective of this contribution is to clarify the impact on acoustical passivity of time-delay in a digital impedance control device, by simple analytical tools and to provide a straightforward remedy to restore acoustical passivity at high frequencies. The structure of the paper allows to follow the natural evolution of the investigations, and the sequentiality of results. After having assessed, in Section 3.1, the effects of both control parameters and time delay on absorption and passivity, an integral constraint has been analytically derived in Section 3.2, incorporating the impacts of each factor on the "waterbed-like" behaviour of the absorption coefficient. It enlarges the integral constraint for purely passive absorbers previously found by [30], toward electro-active resonators. Then, the intimate relationship of acoustical passivity and stability has been clarified by numerical simulations in Section 3.3. A straightforward solution for restoring acoustical passivity (and hence passivity) at high-frequencies is then proposed in Section 3.4. Finally, both passivity and stability outcomes, are validated by experimental tests in Section 4.

2 A model-inversion strategy for impedance control

Our system is a closed box loudspeaker, used as a membrane absorber, thanks to a pressure-based, current driven control architecture [23]. In this configuration, the corrector transfer function between the pressure input and the control variable (the electrical current in the loudspeaker coil) is defined based upon the assumption of knowing the mechanical dynamics of the loudspeaker. The mechanical dynamics assumed for the loudspeaker corresponds to the classical SDOF piston-mode approximation [31], and is reported in Eq. (1).

$$Z_{m0}(s)v(s) = S_d\, p(s) - Bl\; i(s) \tag{1}$$

where s is the Laplace variable, $v(s)$ is the mechanical inward velocity of the loudspeaker diaphragm (check Fig. 1), $p(s)$ is the sound pressure on the diaphragm front face, S_d is the equivalent piston area (also called effective area), Bl is the force factor of the moving coil, $i(s)$ is the current circulating in the moving coil. $Z_{m0}(s)$ is the mechanical impedance of the SDOF loudspeaker model in open circuit configuration, and it writes $Z_{m0}(s) = M_{m0}s + R_{m0} + \frac{K_{m0}}{s}$, where M_{m0}, R_{m0} and K_{m0} are the mechanical mass, resistance and stiffness of the SDOF loudspeaker model respectively. The mechanical stiffness K_{m0} (inverse of compliance C_{m0}) takes into account also the effect of the backing enclosure. In the following stationary regime analysis, s is exchangeable with $\mathrm{j}\omega$, where $\omega = 2\pi f$ is the angular frequency (in rad/seconds) and f is the ordinary frequency (in Hz).
As we are interested in the acoustic behaviour, it is more convenient and intuitive to divide all

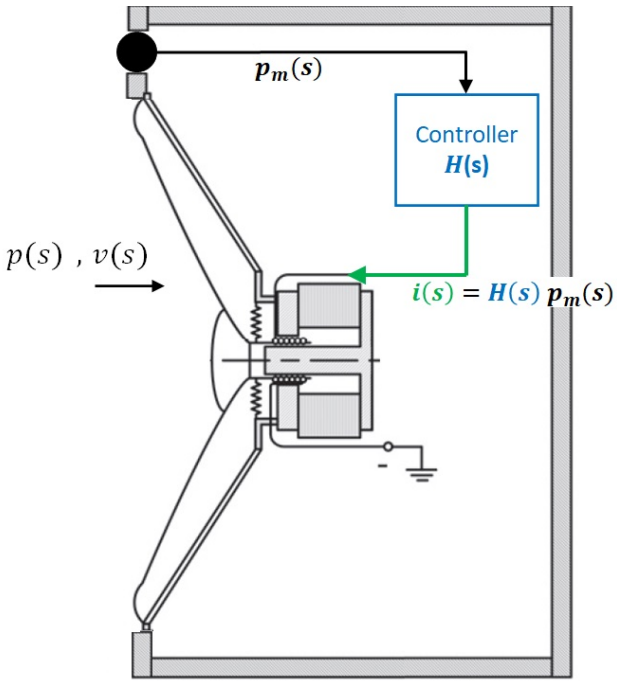

Figure 1. Schematic representation of the closed-box electrodynamic loudspeaker. $p(s)$ and $v(s)$ are the acoustic pressure and inward velocity, respectively, on the speaker diaphragm; $i(s)$ is the electrical current in the loudspeaker coil; $H(s)$ indicates the operator relative to the controller, which applies to the measured pressure $p_m(s)$.

Thiele-Small parameters	M_{m0}	R_{m0}	K_{m0}	Bl	S_d
Units	kg	$\mathrm{N.sm^{-1}}$	$\mathrm{m.N^{-1}}$	$\mathrm{N.A^{-1}}$	$\mathrm{m^2}$
Values	4.45×10^{-4}	0.173	3.85×10^{3}	1.10	1.30×10^{-3}

Table 1. Thiele-Small parameters of the EA.

the terms of Eq. (1) by S_d so that to obtain:

$$Z_{a0}(s)v(s) = p(s) - \frac{Bl}{S_d}\, i(s), \tag{2}$$

where $Z_{a0}(s) = M_{a0}s + R_{a0} + \frac{K_{a0}}{s}$ is the acoustical impedance of the EA in open circuit. Looking at Eq. (2), and supposing that the pressure measured by the microphone $p_m(s)$ be equal to the pressure on the speaker diaphragm, it is easy to derive the transfer function $H(s)$ between $p(s)$ and $i(s)$, in order to achieve a target impedance $Z_{at}(s)$ on the loudspeaker diaphragm, see Eq. (3):

$$H(s) = \frac{i(s)}{p(s)} = \frac{S_d}{Bl}\left(1 - \frac{Z_{a0}(s)}{Z_{at}(s)}\right) \tag{3}$$

The so-called Thiele-Small parameters appearing in Eq. (1) and (3) must therefore be estimated with some technique, taking advantage of electrical and/or acoustic measurements in different configurations [25]. The Thiele-Small parameters of the EA taken into account for the following simulations are reported in Table 1. The natural frequency f_0 of the open-circuit loudspeaker resonator is about 468 Hz.
This is the model-inversion technique employed in [23].

We remind that the model of Eq. (1) corresponds to the piston mode approximation, and higher order mechanical modes of the loudspeaker are not taken into account in the control

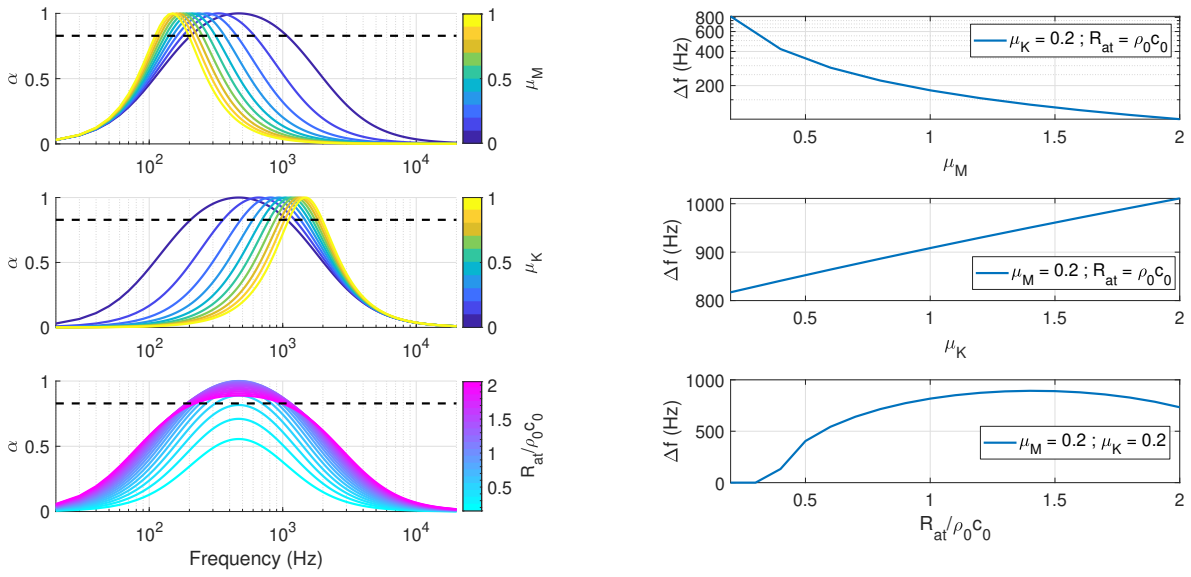

(a) **(b)**

Figure 2. Variation of the normal absorption coefficient $\alpha(\omega)$ (**a**) and absolute bandwidth Δf of efficient absorption (**b**) with respect to each of the target impedance parameters μ_M, μ_K and R_{at}. The default values are $\mu_M = 0.2$, $\mu_K = 0.2$ and $R_{at} = \rho_0 c_0$ respectively.

law (3). This can lead to spill-over effects, which also can contribute to the stability of the entire system. Nevertheless, in this contribution we focus on the effect of the time-delay, and the piston-mode approximation of Eq. (1) is considered as representing the full dynamics of the loudspeaker in our simulations.

The objective of [23] was to attain an acoustic resistance on the loudspeaker diaphragm in an as-wide-as-possible frequency range. The target impedance $Z_{at}(s)$ was then chosen as a target resistance R_{at} equal to the characteristic impedance of air $\rho_0 c_0$ (ρ_0 being the air density and c_0 the air speed in standard atmospheric conditions) to have perfect absorption for normally incident plane waves. In other applications, such as the lining configuration in duct acoustics, or room acoustics, the optimal value for R_{at} becomes a more difficult choice (see [9] and [25]). In any case, a Z_{at} simply equal to the target resistance R_{at}, would bring a non-proper [32] transfer function $H(s)$, and indefinitely increasing current at lower and higher frequencies. Therefore, for causality and energy limits, in the expression of $Z_{at}(s)$ a reactive part was added to R_{at}, see Eq. (4).

$$Z_{at}(s) = M_{at}s + R_{at} + K_{at}/s \tag{4}$$

where M_{at} and K_{at} are the target mass and resistance. Such terms can be written in terms of the acoustic mass and stiffness of the EA in open circuit: $M_{at} = \mu_M M_{a0}$ and $K_{at} = \mu_K K_{a0}$. By doing so, the coefficients μ_M and μ_K indicate how far the target acoustical mass and stiffness differ from the case of open circuit. By varying their ratio, it is possible to set the resonance frequency f_{at} of $Z_{at}(s)$ at different values than the open-circuited EA natural frequency f_0, see Eq. (5). Observe that other target impedances could be employed, as corresponding to a multi-degree-of-freedom resonator [25], and/or with in-parallel components.

$$f_{at} = \sqrt{\frac{\mu_K}{\mu_M}} f_0 = \sqrt{\frac{\mu_K}{\mu_M}} \frac{1}{2\pi} \sqrt{\frac{K_{m0}}{M_{m0}}} \tag{5}$$

The influence of each tunable parameter μ_M, μ_K and R_{at} of the target impedance (4) on the

normal absorption coefficient α are simulated on Fig. 2a. The normal absorption coefficient is given by:

$$\alpha = \frac{4\ \mathrm{Re}\{Y_a(\mathrm{j}\omega)\}\rho_0 c_0}{|1 + Y_a(\mathrm{j}\omega)\rho_0 c_0|^2}, \tag{6}$$

where $Y_a(\mathrm{j}\omega)$ is the acoustical mobility of the EA, supposed here equal to $1/Z_{at}(\mathrm{j}\omega)$. The nominal values for the control parameters are set to $\mu_M = \mu_K = 0.2$ and $R_{at} = \rho_0 c_0$ as representing a possible target of desirable bandwidth. The parametric variation of the absolute bandwidth of efficient normal absorption is simulated in Fig. 2b. The absolute bandwidth Δf in Fig. 2b is the frequency range such that $\alpha \geq \alpha_{th}$, where $\alpha_{th} = 1 - (\sqrt{2} - 1)^2$ corresponds to the case where the total sound intensity on the loudspeaker diaphragm is less than twice the sound intensity of the normal incident wave [25]. From Fig. 2 we can notice that the main impact on the bandwidth is given by the μ_M coefficient, i.e. by the mass term, as the bandwidth significantly enlarges when μ_M is reduced. Despite what was reported in [25] and [23], we remark that also μ_K affects the efficient absorption bandwidth. Concerning R_{at} there is an optimal value (which is more than $\rho_0 c_0$) achieving the largest bandwidth.

Ideally, the impedance on the loudspeaker diaphragm realised by the controller (3) is exactly the target impedance $Z_{at}(s)$. However, this is never the case because of model uncertainties (errors or changes in the Thiele-Small parameters), dynamic uncertainties (neglected modes) and time delay in the digital-based control chain. In this contribution we focus on the effect of the time delay.

3 Simulations

3.1 Time delay and passivity

As any digital control system, a certain time delay happens between the input and the output of the control loop. A total delay τ between the measured pressure and the current in the loudspeaker coil has been estimated to be about 20 microseconds in our implementation of Fig. 1, in accordance with the value reported in [25]. The time delay in the control chain corresponds to an exponential transfer function $e^{-s\tau}$ in the Laplace domain, multiplying the controller $H(s)$ of Eq. (3). Supposing $p_m(s) = p(s)$, the transfer function between the input pressure $p(s)$ and the output diaphragm velocity $v(s)$ is given by Eq. (7).

$$Y_a(s) = \frac{v(s)}{p_m(s)} = \frac{1}{Z_{m0}(s)}\left(S_d - Bl\ H(s)\ e^{-s\tau}\right) \tag{7}$$

Because of the time delay, the acoustic mobility $Y_a(s)$ achieved on the loudspeaker diaphragm is different from the target one ($1/Z_{at}(s)$). In particular, time delay introduces a phase shift multiplying the corrector, which increases in frequency.

Fig. 3 shows the effect of time delay on the normal absorption coefficient and on the mobility phase. The high frequency phase shift of time delay causes the phase of mobility to exit the limits of $[-90°, 90°]$ which assure passivity of a locally-reacting surface. A locally-reacting surface can be defined as passive if the $\mathrm{Re}\{Y_a(\mathrm{j}\omega)\}$ is positive [33], that is if $\alpha(\omega) \geq 0$ for every ω. A negative absorption indicates that more acoustic energy is reflected than the incident one (the reflection coefficient becomes $|R(\mathrm{j}\omega)| \geq 1$). The ratio of the energy injected by a non-passive locally reacting surface, to the incident one, at a certain frequency ω, is given by the negative value of $\alpha(\omega)$.
Higher delay shifts the frequency of loss of acoustical passivity toward lower values, meanwhile

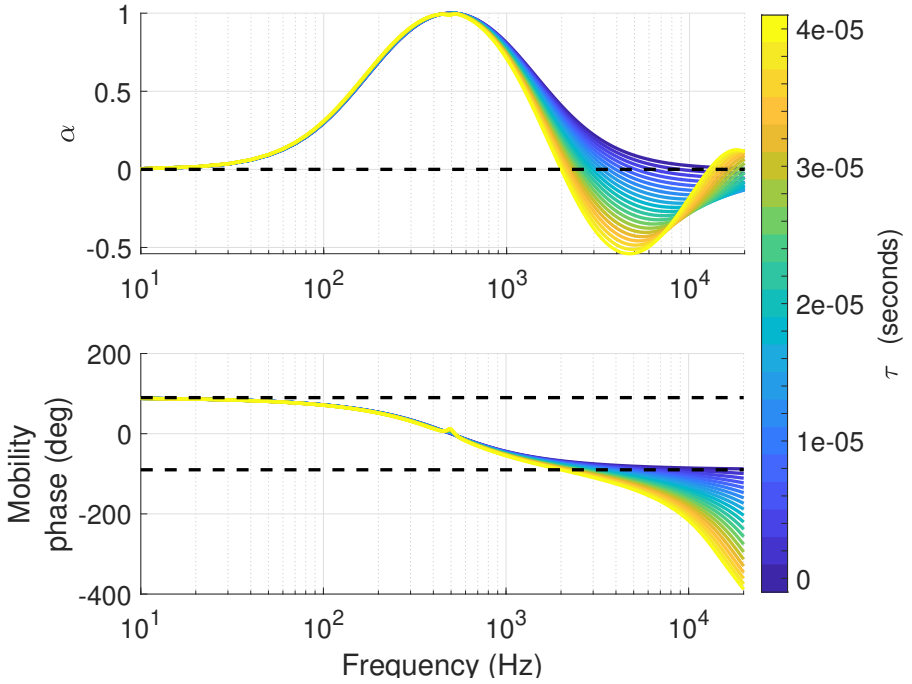

Figure 3. Absorption coefficient α and mobility phase with varying time delay. The target impedance parameters are set to $\mu_M = 0.2$, $\mu_K = 0.2$ and $R_{at} = \rho_0 c_0$.

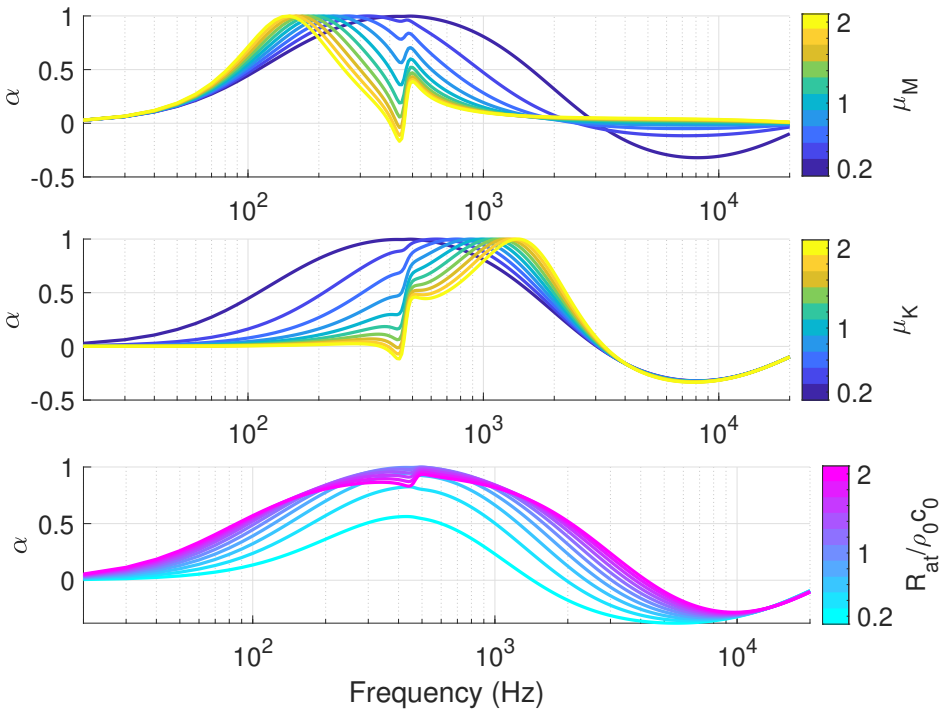

Figure 4. Variation of the absorption coefficient α with respect to the control parameters, in case of a delay in the control loop equal to $\tau = 2 \times 10^{-5}$ seconds. The default values chosen for the control parameters are $\mu_M = 0.2$, $\mu_K = 0.2$ and $R_{at} = \rho_0 c_0$.

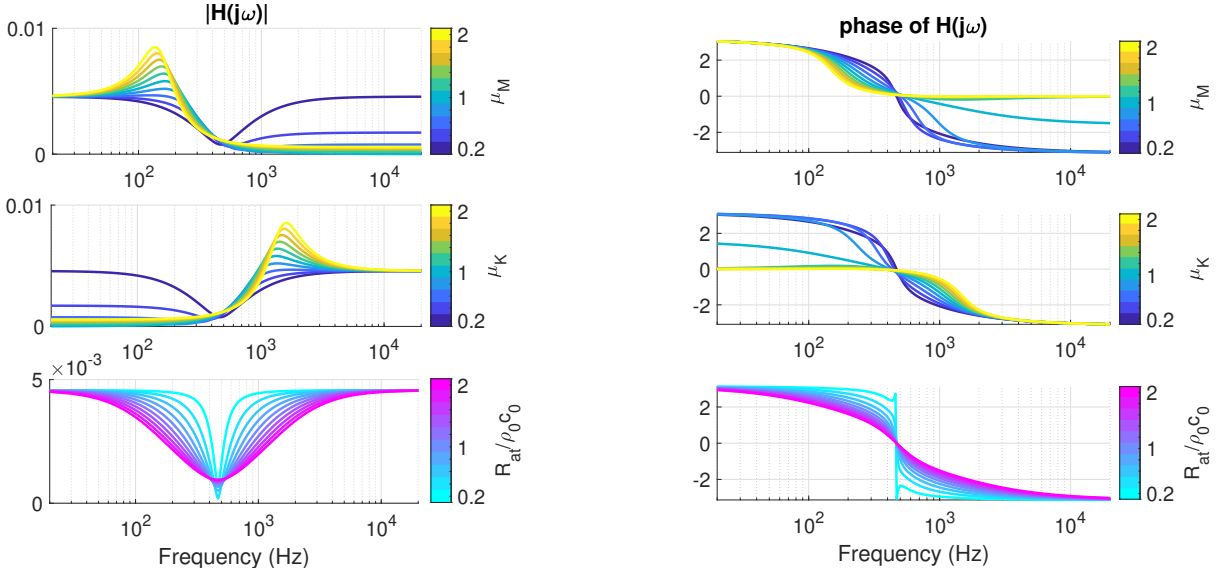

Figure 5. Modulus (**a**) and phase (**b**) spectra of $H(s)$ with varying target impedance parameters.

enhancing the negative drop of $\alpha(\omega)$.
In Fig. 4, the effect of varying the target impedance parameters is presented in case of a time delay of 2×10^{-5} seconds. This value of τ has been estimated in the FEMTO-st Institute of Besançon, France, for the EA tested in Section 4. Fig. 4 shows that, apart from the decay of α at high frequencies, time delay also produces a drop around f_0 as more important as farther we push f_{at} away from f_0. Hence, time delay impacts the performance of such impedance control in two ways, which should be analysed separately. The loss of acoustical passivity around f_0, for f_{at} sufficiently distant from f_0, is caused by a residual open circuit dynamics of the EA. The presence of time delay, indeed, hinders a perfect model-inversion at f_0. Such undesired behaviour could be reduced by properly designed *compensators* [34], as more efficiently as the time delay gets better identified, along with the loudspeaker model.

The high-frequency loss of acoustical passivity on the other hand, caused by the dephasing introduced by τ, gets more severe as lower is the phase of $H(s)$. Fig. 5b clearly correlates with Figure 4, as the high-frequency behaviour is concerned. Apparently, reducing the target mass or resistance significantly diminishes the high-frequency phase of $H(s)$, and hence endangers high-frequency passivity of the delayed control system. Reminding that the best way to enlarge the frequency bandwidth is by reducing μ_M, we conclude that the frequency bandwidth requirement conflicts with the passivity demand. Instead, reducing the target stiffness or increasing the target mass, i.e. shifting the resonance of $Y_{at}(s)$ at lower frequencies, is beneficial for high-frequency passivity.

The physically intuitive concept of acoustical passivity implicitly assumed, is that a system is passive if it absorbs energy, i.e., in our case, if the normal absorption coefficient is positive. We note that the sign of the absorption coefficient depends exclusively on the sign of the real part of mobility, see Eq. (6). Observe that if the normal absorption coefficient is positive, it stays positive for any angle of the incident pressure field [35], therefore it is a property which is fully independent of the external acoustic field, but only depends upon the intrinsic behaviour of the absorber itself.
It is interesting to remark that this acoustical passivity condition is totally equivalent to the *passivity* definition in control theory [13], where a Single-Input-Single-Output (SISO) system is defined as passive if the real part of its transfer function is positive. In our acoustic parallel, a

positive real part of the mobility transfer function $Y_a(\mathrm{j}\omega)$ corresponds to a positive value of the normal absorption coefficient, or also to an absolute value of the normal reflection coefficient (which is nothing less than a bilinear transform [36] of the acoustical mobility) lower than one. The minimum value of the absorption coefficient can be adopted as a *passivity index*, for an acoustic controlled impedance, analogously to the "Input-Feedforward-Passivity" (IFP) index defined in [29]. From the definition of [29], a system is said to have an "excess of passivity" or a "shortage of passivity" if such index is positive or negative respectively.

In order to avoid the *passivity shortage* around f_0, classical compensators could be employed. Nevertheless, to cope with the high-frequency loss of passivity, classical compensators would only shift the problem toward the forthcoming frequencies, because of an *integral constraint* that such EA architecture must obey, see Section 3.2. Moreover, at high frequencies, other speaker modes appear which are not taken into account in the SDOF loudspeaker model, hence making the high-frequency range hardly controllable.

3.2 Integral constraint on the reflection coefficient of the EA

In order to give a further insight in the EA behaviour, both with respect to passivity and absorptive performance, an integral constraint has been derived in Appendix B. Exploiting the theorems of complex analysis, it is possible to arrive at a relationship between a frequency integral of the normal reflection coefficient spectrum $R(\mathrm{j}\omega)$, the open-circuit acoustical stiffness of the speaker K_{a0}, the static corrector transfer function $H(s \to 0)$, and the "unstable zeros" [32] of the reflection coefficient transfer function $R(s)$, i.e. the zeros of $R(s)$ with positive real part. The relationship derived in Appendix B is reported below:

$$-\int_0^\infty \frac{1}{\omega^2} \ln|R(\mathrm{j}\omega)| d\omega = \frac{\pi \rho_0 c_0}{K_{a0}} \left(1 - \frac{Bl}{S_d} \lim_{s\to 0} H(s)\right) - \pi \sum_n \frac{\mathrm{Re}\{s_n\}}{|s_n|^2}, \tag{8}$$

where s_n are the unstable zeros of the normal incidence reflection coefficient transfer function $R(s)$. For $\lim_{s\to 0} H(s) = 0$ we retrieve the integral constraint for purely passive absorbers provided by Yang [30] and reported in Eq. (9).

$$-\int_0^\infty \frac{1}{\omega^2} \ln|R(\mathrm{j}\omega)| d\omega = \frac{\pi \rho_0 c_0 d}{B_{eff}} - \pi \sum_n \frac{\mathrm{Re}\{s_n\}}{|s_n|^2}, \tag{9}$$

where the acoustic stiffness of the loudspeaker in the open-circuit configuration K_{a0} is substituted by the effective bulk modulus B_{eff} divided by the thickness of the sample d. Imposing the acoustical passivity condition, then $-\int_0^\infty \frac{1}{\omega^2} \ln|R(\mathrm{j}\omega)| d\omega = |\int_0^\infty \frac{1}{\omega^2} \ln|R(\mathrm{j}\omega)| d\omega|$ (because $|R(\mathrm{j}\omega)| \leq 1$). Since $\mathrm{Re}\{s_n\} \geq 0$, a constraint on the minimum thickness for a fixed bandwidth of efficient absorption was derived [30]:

$$d \geq \frac{B_{eff}}{\pi \rho_0 c_0} \left| \int_0^\infty \frac{1}{\omega^2} \ln|R(\mathrm{j}\omega)| d\omega \right|. \tag{10}$$

Analogously, for a SDOF-in-series resonator which is purely passive, or having a null static controller $H(s \to 0) = 0$, there is a minimum value of the acoustical compliance needed in order to achieve a certain bandwidth of efficient absorption:

$$C_{a0} = \frac{1}{K_{a0}} \geq \frac{1}{\pi \rho_0 c_0} \left| \int_0^\infty \frac{1}{\omega^2} \ln|R(\mathrm{j}\omega)| d\omega \right|. \tag{11}$$

Eq. (10) and (11) imply that high absorption in purely passive absorbers (such as porous materials or Helmholtz and quarter-wavelength resonators) is not possible for any finite thickness

or finite compliance, especially at lower frequencies (look at the expression of the integrand) if not for narrow peaks [30].
If the pressure-based, current-driven control architecture is applied to a SDOF-in-series resonator like a loudspeaker instead, Eq. (8) holds. If the controller is supposed to keep the acoustical passivity of the system, then once again $-\int_0^\infty \frac{1}{\omega^2}\ln|R(\mathrm{j}\omega)|d\omega = |\int_0^\infty \frac{1}{\omega^2}\ln|R(\mathrm{j}\omega)|d\omega|$, and we get:

$$-H(0) \geq \frac{S_d}{Bl}\frac{K_{a0}}{\pi\rho_0 c_0}\left|\int_0^\infty \frac{1}{\omega^2}\ln|R(\mathrm{j}\omega)|d\omega\right|. \tag{12}$$

Therefore, $H(0)$ must be a negative real number with a minimum absolute value depending upon the frequency bandwidth of efficient absorption and upon the acoustic stiffness K_{a0} of the passive resonator under control, as well as the ratio S_d/Bl. Indeed, $-H(0)S_d/Bl$ is the contribution of the control architecture on the loudspeaker first mode compliance term. This means that, for any acoustic stiffness (or compliance) of the passive resonator, if the acoustical passivity of the resonator with the control applied is kept, then a minimum amount of electrical current is required at the static limit. In case of the control transfer function (3), $H(0) = Sd/Bl(1-1/\mu_K)$. This is in agreement with what stated in Section 3.1, as in order to keep high frequency passivity, the operative bandwidth should shift toward lower frequencies (increasing μ_M or reducing μ_K for the SDOF target impedance), which entails higher electrical current supply at the static limit (see Fig. 5a). Note that such integral constraint holds for any corrector $H(s)$ which is a proper and stable rational transfer function.
From the integral constraint (8), it is clear that there is a strong relationship between the frequency bandwidth of efficient absorption, the low-frequency controller transfer function (which means electrical energy supply), and the acoustical passivity. In order to visually interpret the significance of such integral relationship, let us assign the letters A, B and C to the three contributions appearing in Eq. (8), i.e.:

- $A = -\int_0^\infty \frac{1}{\omega^2}\ln|R(\mathrm{j}\omega)|d\omega$,
- $B = \frac{\pi\rho_0 c_0}{K_{a0}}\left(1 - \frac{Bl}{S_d}\lim_{s\to 0} H(s)\right)$,
- $C = \pi\sum_n \frac{\mathrm{Re}\{s_n\}}{|s_n|^2}$,

such that Eq. (8) becomes $A = B - C$.
In Fig. 6a, each term of the integral equation (8) is plotted with varying time delay τ from 0 to 4×10^{-4} seconds, the control parameters being fixed to $\mu_M = \mu_K = 0.2$ and $R_{at} = \rho_0 c_0$. The dashed black line is the right hand side (rhs) of Eq. (8) ($B-C$ in Fig. 6a), which must coincide with the left hand side of Eq. (8) (called A in Fig. 6a). Apparently, increasing the time delay brings about unstable poles of the reflection coefficient of larger real parts, increasing the term C in Fig. 6a. Fig. 6b allows to verify that higher τ produces unstable zeros of $R(s)$ with larger real parts. As the static transfer function $H(0)$ does not vary if μ_K is fixed, the term called B in Fig. 6a is unchanged. Hence, higher time delays reduce $B-C$. In this perspective, Fig. 3 can be reinterpreted as a direct consequence of the integral constraint (8). Indeed, as higher time delays reduce $B-C$, for a fixed operative bandwidth where $\alpha > \alpha_{th}$ (i.e. fixed control parameters μ_M,μ_K and R_{at}), the high frequency absorption coefficient α must be negative and of larger modulus so that to negatively contribute to the overall frequency integral A, and satisfy the equality $A = B - C$.

Figs. 7, 8 and 10 present the variation of each term of the integral constraint (42) with the control parameters, in case of perfectly synchronous **(a)** and time-delay affected ($\tau = 2\times10^{-5}$

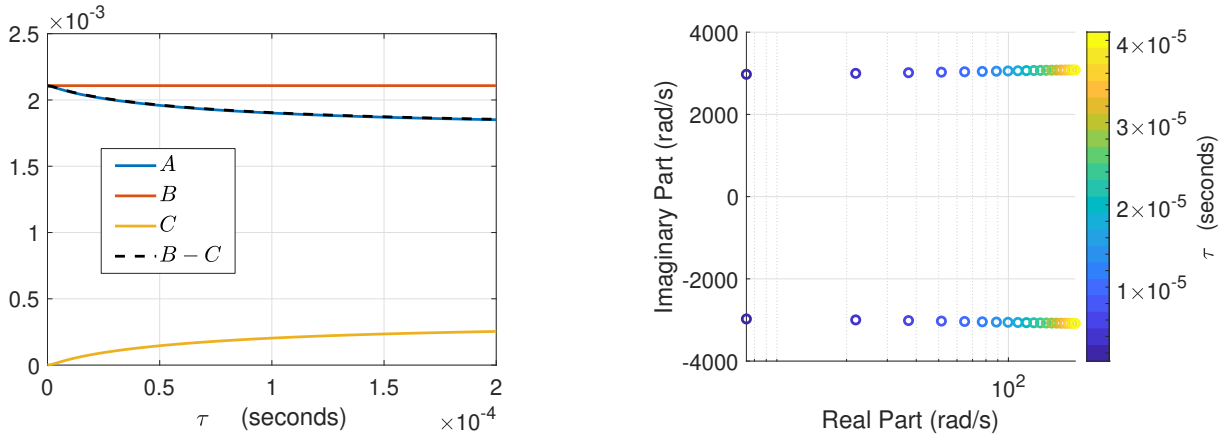

(a) **(b)**

Figure 6. Plot of each term of the integral equation (8) (left) and of the unstable zeros of $R(s)$ with positive real part, with varying time delay τ from 0 to 2×10^{-4} seconds. The control parameters are set to $\mu_M = \mu_K = 0.2$ and $R_{at} = \rho_0 c_0$.

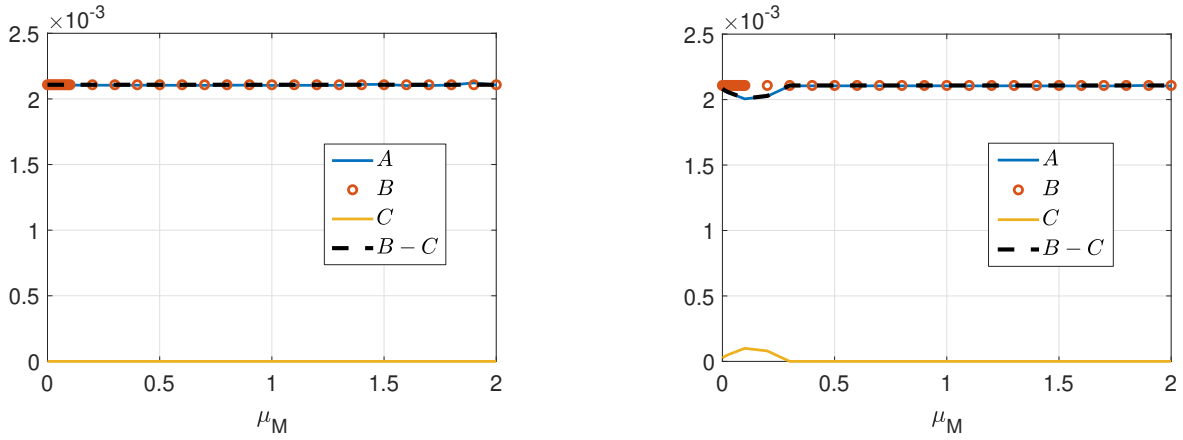

(a) **(b)**

Figure 7. Plot of each term of the integral equation (8), with varying μ_M from 0 to 2, in case of no delay (**a**) and $\tau = 2 \times 10^{-5}$ seconds (**b**). The other control parameters are set to $\mu_K = 0.2$ and $R_{at} = \rho_0 c_0$.

seconds) **(b)** control. The nominal parameters are set to $\mu_M = \mu_K = 0.2$ and $R_{at} = \rho_0 c_0$.
From Figs. 7a, 8a and 9a, we notice that, in case of no-delay and for $R_{at} = \rho_0 c_0$, $R(s)$ has no unstable zeros (the curve C is fixed at 0), irrespective of the values chosen for μ_M and μ_K. The presence of a $\tau \neq 0$ instead, causes the contribution C to be slightly different from 0, for low values of μ_M and/or μ_K.
Hence, Figs. 7, 8 and 9 illustrate that only by reducing μ_K (i.e. increasing $|H(s \to 0)|$) the integral A can be enlarged, as specified by Eq. (12).
Figs. 10 shows that reducing R_{at} below 1 in case of no-delay, and below 1.1 in case of $\tau = 2 \times 10^{-5}$ seconds, creates unstable zeros in $R(s)$, and increases the contribution C, so to further constraining the integral A.

Fig. 7 to 10 verify that the identity (42) holds for any values chosen for μ_M, μ_K and R_{at}. The integral relationship (8) is another means for the understanding and design of the EA control based upon the specifications assigned. For example, adding phase-lead or lead-lag compensators at high frequencies, as proposed in [22]), to restore passivity, would inevitably

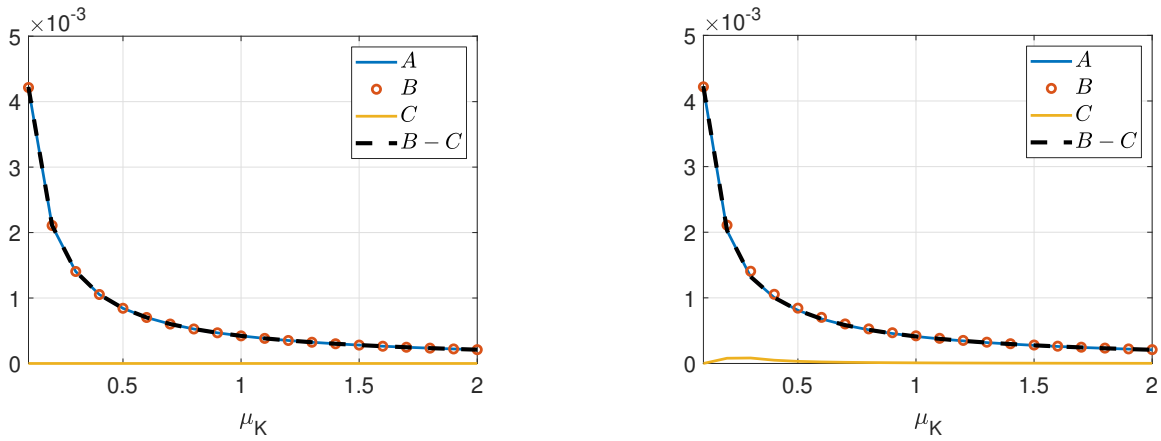

(a) **(b)**

Figure 8. Plot of each term of the integral equation (8), with varying μ_K from 0.1 to 2, in case of no delay (**a**) and $\tau = 2 \times 10^{-5}$ seconds (**b**). The other control parameters are set to $\mu_M = 0.2$ and $R_{at} = \rho_0 c_0$.

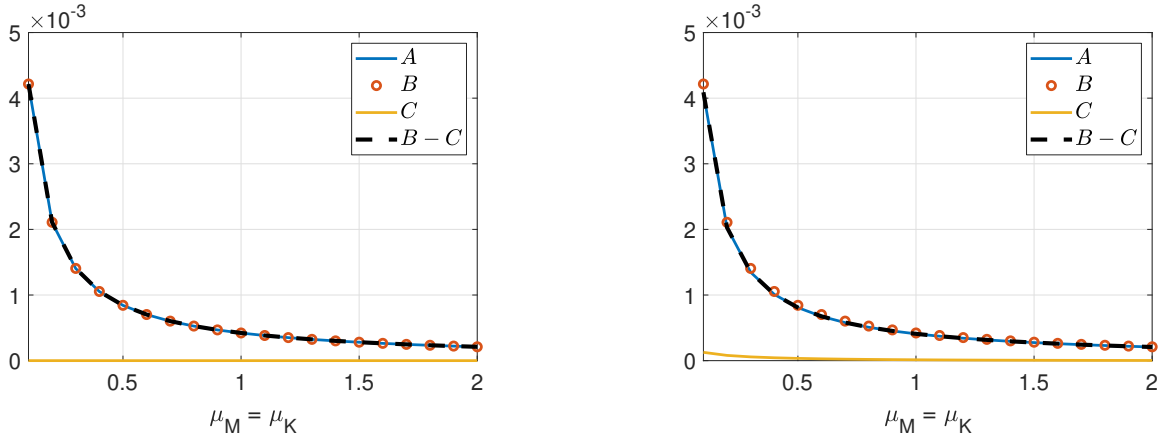

(a) **(b)**

Figure 9. Plot of each term of the integral equation (8), with varying $\mu_M = \mu_K$ from 0.1 to 2, in case of no delay (**a**) and $\tau = 2 \times 10^{-5}$ seconds (**b**). R_{at} is set to $\rho_0 c_0$.

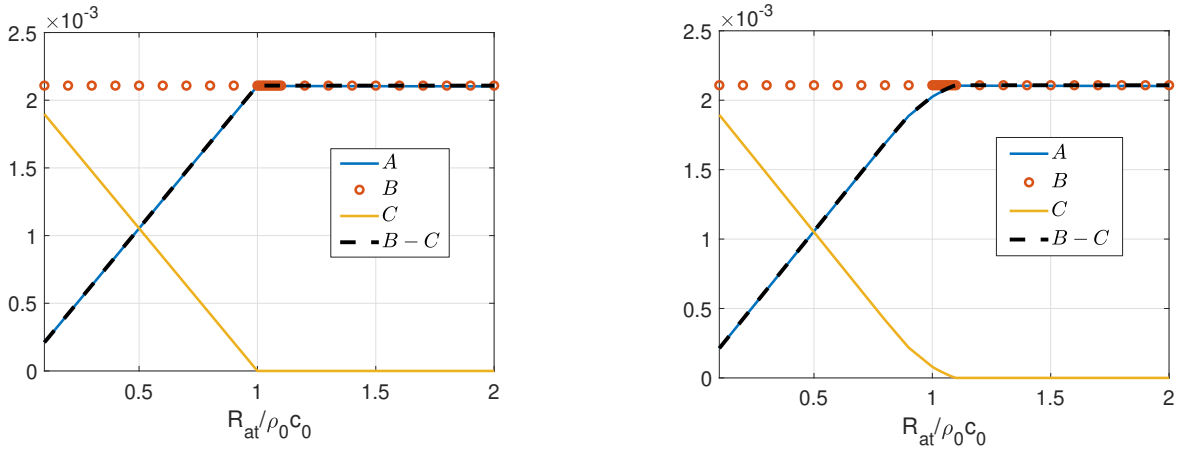

(a) **(b)**

Figure 10. Plot of each term of the integral equation (8), with varying R_{at} from $0.1\rho_0 c_0$ to $2\rho_0 c_0$, in case of no delay (**a**) and $\tau = 2 \times 10^{-5}$ seconds (**b**). The other control parameters are set to $\mu_M = \mu_K = 0.2$.

increase $|H(\mathrm{j}\omega)|$, then reducing the acoustical passivity, at the forthcoming frequencies. Looking at Eq. (8) indeed, it can be verified that a phase lead or lead-lag compensator would increase the term C (augmenting the real part of the unstable zeros of $R(s)$). As the term B is untouched by high-frequency modification of $H(s)$, this would bring about an inevitable reduction of the integral A, which translates into a deeper negative peak of $\alpha(\omega)$ at higher frequencies.
In order to assure the acoustical passivity at high-frequencies, even in the presence of time-delay, $|H(\mathrm{j}\omega)|$ should be quickly cut-down to zero above resonance. In the control law defined by Eq. (3), with the target impedance of Eq. (4), this means that we must increase μ_M and reduce μ_K (see Fig. 2a). A lower μ_K augments $|H(s \to 0)|$ allowing to relax the constraint B on the integral A in the relationship (8). Nevertheless, for higher μ_M, the bandwidth of efficient absorption is significantly narrowed (see Fig. 2b). Hence, we conclude that the control law based upon the SDOF in-series impedance (4) requires a compromise between passivity and operative bandwidth of absorption. Other target impedances might nonetheless be chosen (and are currently under investigation), in order to optimize the bandwidth as well as assuring the high-frequency acoustical passivity, while at the same time respecting the limitation upon the electrical current supply (given by $|H(\mathrm{j}\omega)|$ times the pressure levels involved). This threefold specification might be implemented in an optimization algorithm to synthesize the ideal corrector $H(s)$ which would at the same time produce the required bandwidth of efficient absorption, keep the high-frequency passivity, and respect the constraints on electrical energy demand.
In this and the previous Sections, we have entered into the details of the "water-bed"-like behaviour of the absorption coefficient in case of time delay and its consequences on acoustical passivity, providing useful tools to take it into account for innovative correctors design. In the next section, we clarify the relationship between acoustical passivity and stability. In classical control schemes, indeed, the problem of non-passive systems manifests itself when a feedback is applied between the output and the input. This is also the case here, with the peculiarity that the feedback between the output velocity and the input pressure is given by the acoustic domain in which the controlled loudspeaker is placed. Indeed, as the control system becomes *acoustically active*, the problem of the acoustic feedback, typical of *acoustically*-ANC techniques, comes back into the scenario.

3.3 Time delay and stability

Coupling an acoustically *non-passive* device with a conservative acoustic cavity inevitably leads to instability. In Appendix A, it is briefly recalled the solution of a 1D acoustic hard-walled cavity with a rigid termination on one side, and a generic acoustic element characterized by a reflection coefficient $R(s)$ on the other. It is shown how a reflection coefficient such that $|R(s_p)| > 1$ (where s_p is a pole of the entire system) causes $\mathrm{Re}\{s_p\} > 0$, i.e. instability. Thanks to the simple expression of the radiation impedance in a 1D cavity, in the current section, the stability is analysed by an equivalent approach dearer to control engineers: the poles calculation of the closed-loop transfer function. By evaluating the poles of the closed-loop transfer function of the entire system coupling our EA with a 1D hard-walled rigidly terminated acoustic waveguide, we verify that the effect of each control parameter on the unstable poles is in accordance with the results of Section 3.1.

In Fig. 11 the block diagram relative to the pressure-based, current-driven impedance control is depicted, where $p_m(s)$ is the pressure sensed by the microphone; $v(s)$ and $p(s)$ are, respectively, the velocity and pressure on the loudspeaker diaphragm; $Z_{rad}(s)$ is the radiation impedance of the acoustic domain where the loudspeaker is placed; $\tilde{p}(s)$ and $\tilde{p}_m(s)$ are, respectively, the perturbations upon the pressure on the speaker (due for example to a secondary source), and on the measured pressure (due to measurement noise and/or non-collocation effects) at the microphone location; $Y_{m0}(s)$ is the mechanical mobility of the loudspeaker without control

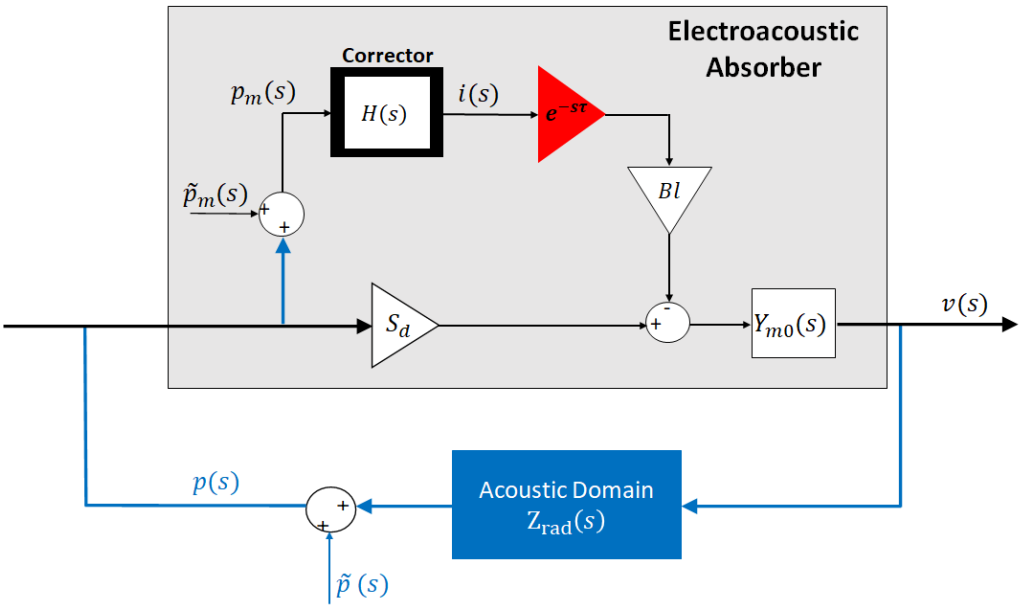

Figure 11. Block diagram of the pressure-based, current-driven impedance control.

$Y_{m0}(s) = 1/Z_{m0}(s)$.
We highlight that it is not possible to incorporate the radiation impedance $Z_{rad}(s)$ into $Z_{m0}(s)$ (as proposed in [23] and [22]), because the transfer function $Z_{rad}(s)$ plays the role of a feedback term in the closed loop of our controlled system.
The system will be stable against perturbations (either on the measurement or on the external field) if the transfer function of the closed loop of Fig. 11 is stable. The closed loop transfer function between the pressure perturbation on the speaker $\tilde{p}(s)$ and the diaphragm velocity is given by Eq. (13):

$$\frac{v(s)}{\tilde{p}(s)} = \frac{Y_a(s)}{1 - Y_a(s)Z_{rad}(s)}, \tag{13}$$

whereas the closed loop transfer function between the pressure perturbation on the measurement $\tilde{p}_m(s)$ and the diaphragm velocity, is $v(s)/\tilde{p}_m(s) = -Y_{a0}(s)BlH(s)e^{-s\tau}/(1 - Y_a(s)Z_{rad}(s))$. In both cases the stability margin is given by the product $Y_a(s)Z_{rad}(s)$ with respect to the unstable point $+1$, as reported in [25]. If the open loop (i.e. open field) transfer function between the measured pressure $p_m(s)$ and the speaker diaphragm velocity $v(s)$ is passive (see Section 3.1 for definition of passivity), being the feedback operator $Z_{rad}(s)$ always passive, then the entire closed loop will also be passive as passivity is preserved under feedback interconnections [13]. Since passivity is a sufficient condition for stability [13], then the closed loop will be unconditionally stable. In the plane wave assumption, the acoustic load relative to a rigidly-terminated hard-walled duct of length L corresponds to the transfer function reported in Eq. (14), which is derived from the plane wave decomposition (see Appendix A), thus supposing to stay below the cut-on frequency of higher order duct-modes in the rigid duct.

$$Z_{rad}(s) = -\rho_0 c_0 \frac{e^{sL/c_0} + R_{term}e^{-sL/c0}}{e^{sL/c0} - R_{term}e^{-sL/c0}}. \tag{14}$$

In the formula of Eq. (14), R_{term} is the reflection coefficient of the termination, which is taken equal to 1 in what follows. In order to analyse the stability, we choose to calculate the poles rather than to evaluate the Nyquist diagram as the latter becomes laboured in case of resonances in the feedback term. The presence of the exponentials in Eq. (13), makes it a transcendental equation. Therefore, for the poles calculation, we need to approximate it with a

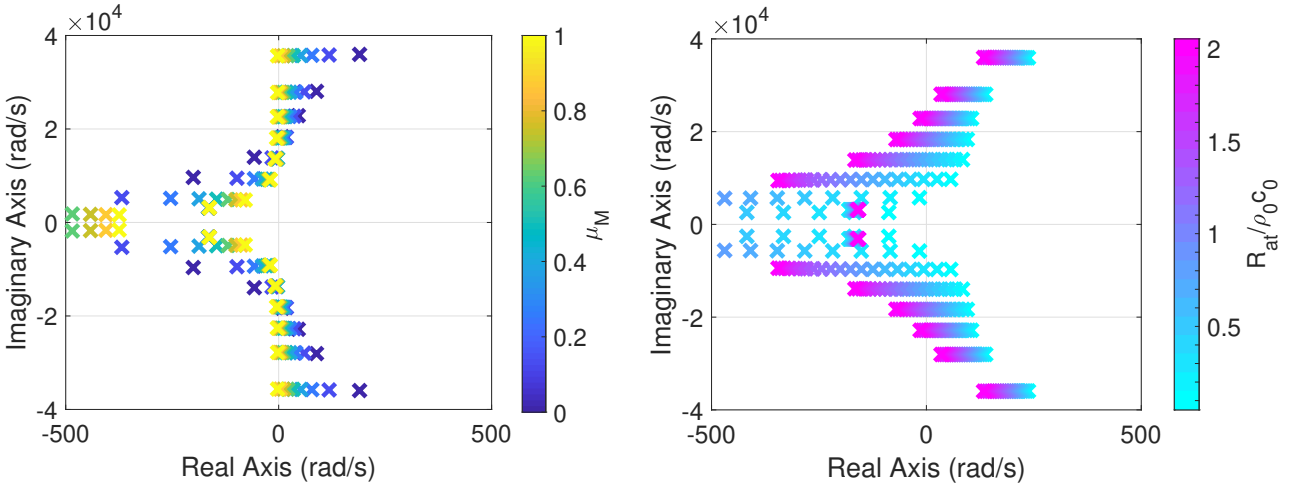

Figure 12. Closed loop poles migration with varying control parameters: μ_M (left), R_{at} (right).

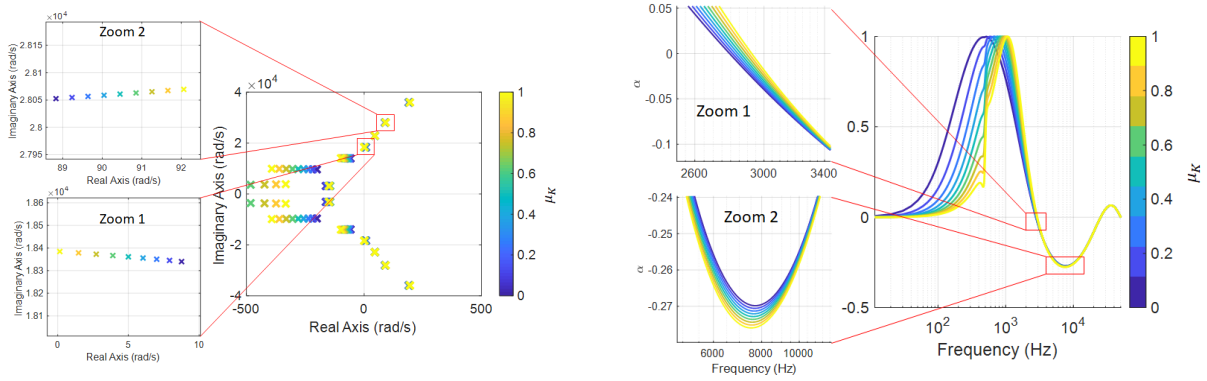

(a) **(b)**

Figure 13. Effect of μ_K on passivity (**a**) and stability (**b**).

rational proper transfer function. In order to do that, it is common practice [29] to approximate the complex exponentials appearing in Eq. (7) and (14) by the Padé ratio of polynomials [37], whose order is adjusted in order to have perfect matching with the actual transfer function in the frequency range of interest.

In Fig. 12 we compute the migration in the complex plane of the poles of the closed loop transfer function (13) with $L = 0.24$ m, by varying the control parameters. The nominal values of μ_M, μ_K and R_{at} are the same as the ones of Section 3.1. From Fig. 12 it is visible how reducing μ_M causes the unstable poles to increase their positive real-part significantly, which means quicker divergence of pressure. Decreasing R_{at} also appreciably move the unstable poles toward the rhp. The effect of reducing μ_K instead is double-sided and is reported in Fig. 13a, along with the absorption coefficient variation in Fig. 13b. Fig. 13a Zoom 1 shows that the smallest unstable pole increases its real part for higher μ_K, whereas the higher unstable poles present opposite tendency (check Fig. 13a Zoom 2). This trend is in accordance with the effect of μ_K on acoustical passivity showed in Fig. 13b.

Hence, the effects of the control parameters on stability are coherent with their effects on passivity presented in Section 3.1.

Both in this section and in Appendix A, we have supposed a conservative acoustic cavity in front of the EA. Similar computations can be carried out by simulating the actual damping present in the cavity, in order to assess whether the coupled system is actually stable or not. In the latter case, an obvious remedy is to add some damping into the system. The next section

propose a simple solution to restore the acoustical passivity of the EA at high frequencies. If we are able to achieve acoustical passivity at any frequency, then the system will be stable whatever the acoustic cavity wherein the EA is placed.

3.4 Acoustic passivation

In order to enlarge the frequency bandwidth without becoming unstable, it is necessary in some way to restore the acoustical passivity at high frequencies. In [38] four general possible *passivation* methods are presented: series, feedback, feedforward and hybrid compensation. These methods are classically used in order to passivate a (non-passive) plant before applying the controller, therefore exploiting the robust stability properties of passivity-based control laws [38]. In our case, it is the entire plant+controller system which has to be acoustically passivated, and it presents a time delay in series with the control itself. Therefore, a series passivation, generally through alternating poles and zeros (such as high frequencies phase-lead or lead-lag compensators, as the ones proposed in [22]) does not solve the problem. Indeed, while allowing passivity over a larger frequency range (leading to what Kelkar calls "Band-Limited Positive Real systems" [38]), a series passivation would bring about a more serious loss of passivity at the higher frequencies, as it is demonstrated by Eq. (8) in Section 3.2. Not even feedback compensation can passivate a non-minimum-phase system [38], and in any case our architecture does not provide for full-feedback control (feedback of both pressure and velocity). A possible solution is a feedforward compensation, that is a transfer function between the input pressure and the output velocity which would add up to the entire system transfer function $Y_a(s)$ [38]. Nevertheless, it is hard, if not impossible, to conceive a feedforward acoustical passivation through an electrical network or controller, acting directly on current without deteriorating the performance at the operating frequencies and, mostly, being devoid of time delay. Predictor-like schemes [34] might be investigated, nevertheless, our SDOF loudspeaker model does not describe the actual dynamics at high frequencies, likely worsening the problem at those regions with spill-over effects. From here, the need to acoustically passivate our system by physically filtering the high-frequencies. Hence, the most straightforward and intuitive solution is to physically apply a porous layer in front of the loudspeaker membrane. Porous materials are renown for their good absorptive properties at high frequencies, allowing to compensate for the *shortage of acoustical passivity* of our EA at those frequencies. In Fig. 14 an example of application of a porous layer in front of the speaker is depicted. The porous layer must be attached on the support of the loudspeaker so that there is never a contact between the speaker's diaphragm in vibration and the porous treatment.
The application of the porous sheet can be seen as a passivation through an input-output transformation matrix M, as the one proposed by Xia et al. [29]. In our case, M is the Transmission Matrix relative to the porous medium described in Eq. (15) where p_1, v_1 are, respectively, the input pressure and output velocity of the EA system, while p_2, v_2 are, respectively, the input pressure and output velocity of the entire EA plus porous layer system (see Fig. 14).

$$\begin{bmatrix} p_2 \\ v_2 \end{bmatrix} = \begin{bmatrix} M_{11} & M_{12} \\ M_{21} & M_{22} \end{bmatrix} \begin{bmatrix} p_1 \\ v_1 \end{bmatrix} = \begin{bmatrix} \cos(k_c d) & -\mathrm{j} z_c \sin(k_c d) \\ -\mathrm{j} z_c^{-1} \sin(k_c d) & \cos(k_c d) \end{bmatrix} \begin{bmatrix} p_1 \\ v_1 \end{bmatrix} \tag{15}$$

The terms of the passivating Transformation Matrix are introduced in the block diagram of Fig. 15, where the EA is represented by its acoustic mobility $Y_a(s)$. Observe that the elements of the transformation matrix for the porous layer, cannot be written as proper transfer functions, therefore limiting the possibility to find an electrical equivalent to the porous passivation.

From Eq. (15), the acoustic impedance of the EA (the cell) with a porous layer in front, can be derived (it is the so-called Impedance Translation Theorem [39]).

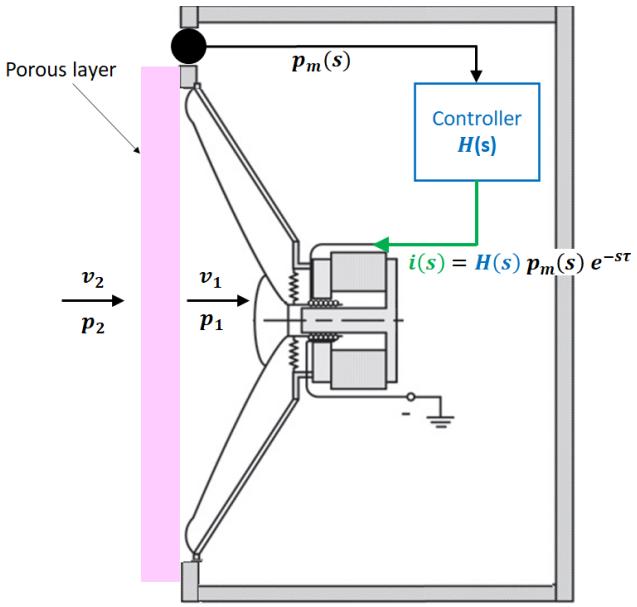

Figure 14. Sketch of the porous layer arrangement on the EA.

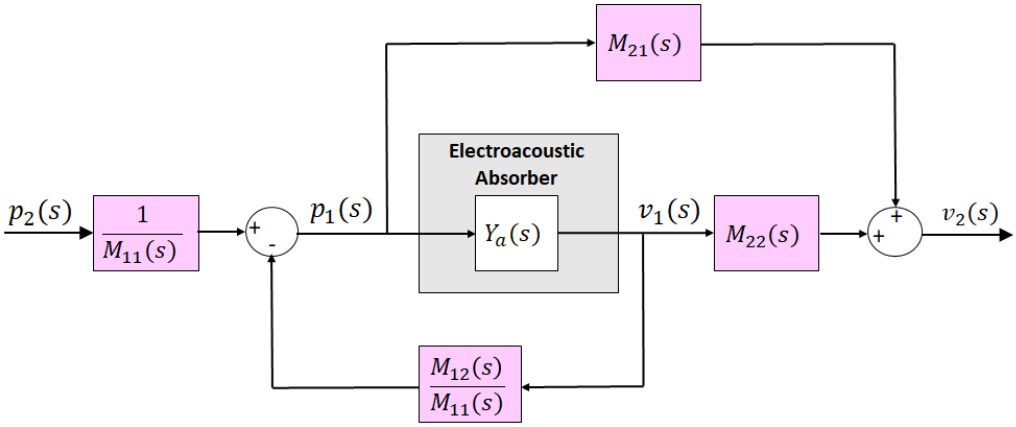

Figure 15. Block diagram of the input-output transformation matrix for passivation applied to our controlled EA.

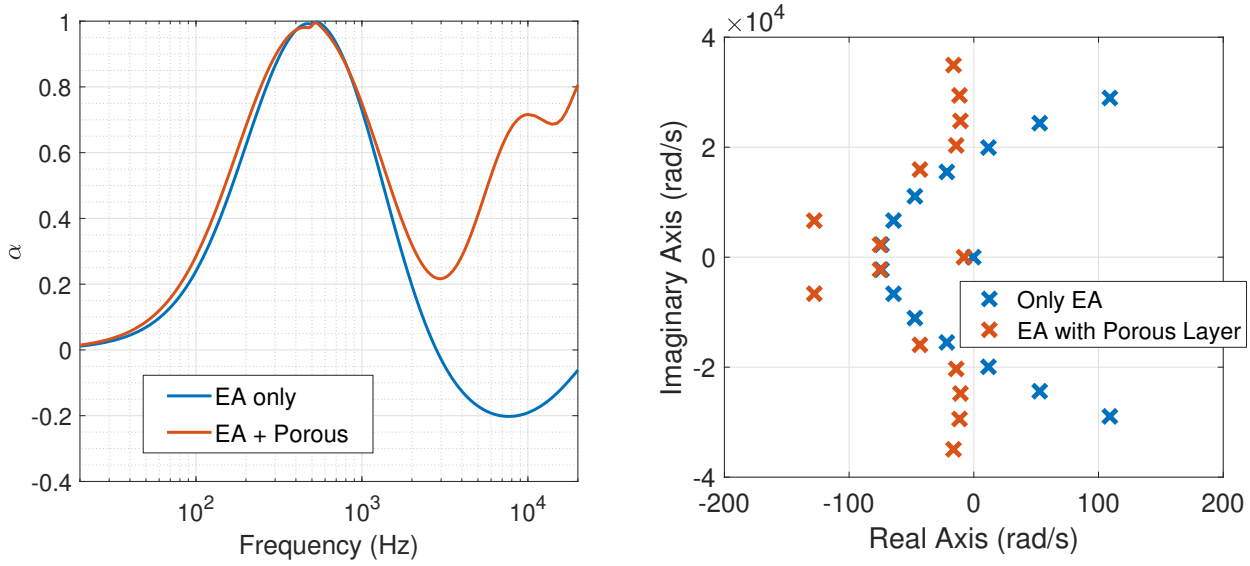

Figure 16. Simulated absorption coefficient (left) and poles of the closed loop transfer function (right), in case of simple EA (blue) and EA plus porous layer (red). The control parameters for the EA are set to: $\mu_M = \mu_K = 0.3$, $R_{at} = \rho_0 c_0$. The porous layer has a thickness of 12 mm and flow resistivity $\sigma = 1 \times 10^4$ rayl/m.

$$Z_2(\mathrm{j}\omega) = \frac{p_2(\mathrm{j}\omega)}{v_2(\mathrm{j}\omega)} = z_c(\mathrm{j}\omega)\frac{\mathrm{j}Z_1(\mathrm{j}\omega)\cot(k_c(\mathrm{j}\omega)d) + z_c(\mathrm{j}\omega)}{Z_1(\mathrm{j}\omega) - \mathrm{j}z_c(\mathrm{j}\omega)\cot(k_c(\mathrm{j}\omega)d)} \tag{16}$$

where $Z_2(\mathrm{j}\omega)$ is the acoustic impedance of the EA with porous layer applied; $Z_1(\mathrm{j}\omega) = 1/Y_a(\mathrm{j}\omega)$ is the acoustic impedance of the EA without porous layer; $k_c(\mathrm{j}\omega)$ and $z_c(\mathrm{j}\omega)$ are the wave number and the characteristic impedance of the porous medium in the equivalent-fluid modelling [39], here obtained by the Miki semi-empirical power laws [40] based upon the flow resistivity.

In Fig. 16 we simulate the normal absorption coefficient (on the left) and the poles of the closed loop transfer function (on the right) of the EA (in blue) and of the EA with a porous layer applied (in red). The porous layer considered here, has thickness $d = 1.2$ cm and flow resistivity $\sigma = 1 \times 10^4$ rayl/m, as a typical value for foams. The mobility of the EA with porous layer applied $Y_2(\mathrm{j}\omega) = 1/Z_2(\mathrm{j}\omega)$ has a transcendental expression, thus $Y_2(\mathrm{j}\omega)$ has been substituted by a proper rational transfer function which perfectly fits the actual $Y_2(\mathrm{j}\omega)$ in all the frequency range of interest (not shown here), in order to evaluate the poles of the closed loop transfer function of Eq. (13) (in Eq. (13) read $Y_2(s)$ instead of $Y_a(s)$ in case of porous layer applied).

From the simulations of Fig. 16, the porous sheet has the effect of restoring the passivity and therefore the stability, without practically affecting the performance of the EA in the operating frequency range (around the resonance of the loudspeaker).

We remind that the higher the delay, or the lower the μ_M or R_{at} parameters, the more serious will be the *shortage of passivity*. Therefore, to attain full passivation (to re-establish a positive "passivity index" [29]), we need a more performant (in terms of high frequency absorption) porous layer, which usually means a thicker sample and/or a higher flow resistivity. Another possible improvement for the acoustic passivation, is to add a thin air-gap between the EA and the porous layer, so as to increase high frequency viscous dissipation at the porous location [39] at certain frequencies, as simulated in Fig. 17. To calculate the resulting acoustic impedance in front the porous layer, the Impedance Translation Theorem has been applied recursively as described in [39]. The air-gap thickness is an additional variable which could be adjusted for the optimal design of the acoustic passivation. Fig. 17 also shows the effect

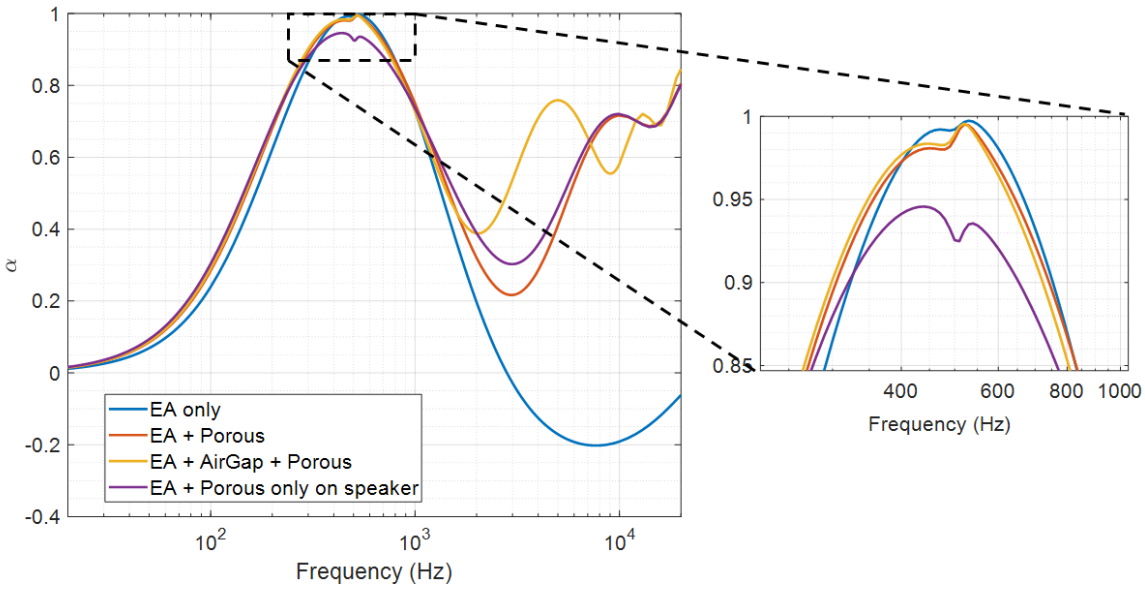

Figure 17. Simulated normal absorption of the EA only (in blue), of the EA plus a porous layer (in red), of the EA plus a porous layer with a 1 cm air-gap between them, and in case of porous layer applied just on the speaker (see Appendix C). The EA control parameters are: $\mu_M = \mu_K = 0.2$, $R_{at} = \rho_0 c_0$; the porous layer thickness considered is 12 mm with a flow resistivity $\sigma = 1 \times 10^4$ rayl/m.

of placing the porous layer just in front of the speaker (and not in front of the microphones). The analytical derivation of the corresponding equivalent impedance is reported in Appendix C. Apparently, α is significantly affected at the resonance. This result will help in the interpretation of the experimental curves reported in Section 4. In Appendix C, the effect of varying the flow resistivity σ is also displayed, showing how the porous layer should be carefully chosen in order not to degrade the performance of the EA, or even endanger acoustical passivity in the operative bandwidth.

We underline that this passivation technique should not be confused with a hybrid impedance control as the one proposed by [8], because in our case the porous element has the only scope of restoring passivity at high frequencies, and it should not (directly) affect the performance of the EA around the targeted bandwidth of absorption.

4 Experimental tests

In this section, the EA is experimentally tested in order to verify the effect of the time delay on passivity and stability simulated in the previous sections. In Fig. 18 there is a picture of the EA produced in FEMTO-ST Institute, Department of Applied Mechanics. The EA is composed by a loudspeaker and four microphones at the corners used to estimate an average pressure on the speaker diaphragm. The back case accommodates the necessary electronics for the control. In Fig. 18 on the right, a layer of 12 mm of melamine foam is applied in front of the loudspeaker (but not in front of microphones), in keeping with the sketch of Fig. 14. Fig. 19 shows the Howland current pump circuit [24] adopted in the EA for the current-driven control. It retrieves the one proposed in [23], including an operational amplifier, two input resistors R_i, two feedback resistors R_f, and a current sense resistor R_s. The resistance R_d and capacitance C_f constitutes the compensation circuit to ensure stability with the grounded load [41]. The corrector transfer function $H(s)$ is digitally implemented by the Infinite Impulse Response technique (IIR) [42], through a programmable digital signal

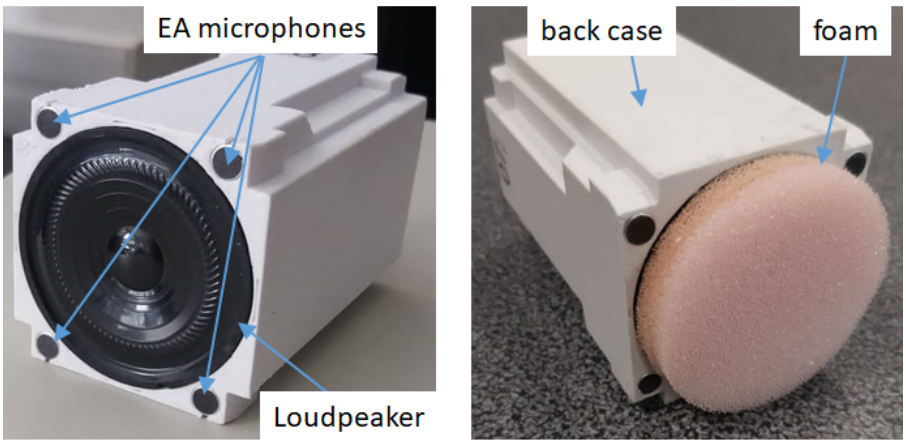

Figure 18. Our EA, before (left) and after (right) the application of the porous layer.

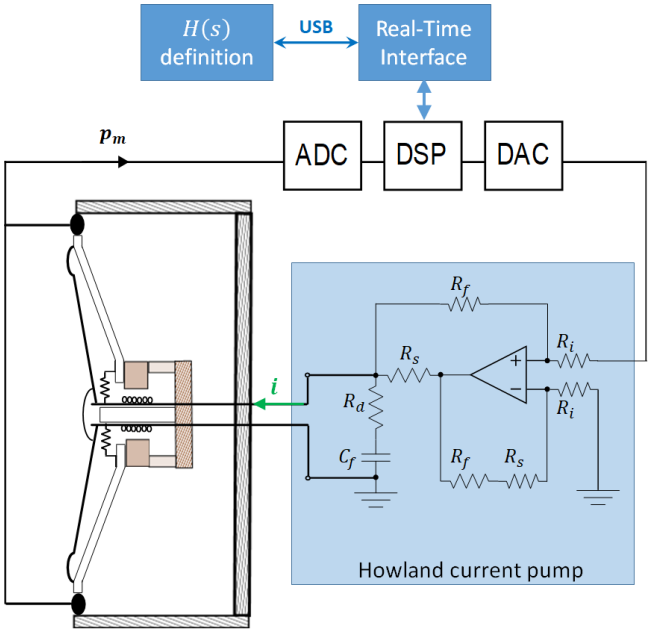

Figure 19. Scheme of the electronic components of the EA control.

processor (DSP) specifically designed for the EA in the FEMTO-st Institute, as presented in [43].

In Fig. 20, the Kundt's tube adopted for the normal absorption measurements is photographed. The tube is made by plexiglass and supposed rigid, it is 60 cm long and has a squared cross-section of $D = 53$ mm side (cut-on frequency $f_{cut-on} = c_0/2D = 3.2$ kHz). The two microphones for the Two-Microphone Method (2MM) [44] are spaced by 4 cm along the tube and the distance between the EA and the centre of the closest microphone is 28 cm. The source is an external loudspeaker reproducing a swept-sine noise signal from 150 Hz to 3.2 kHz, which are the lower and upper limits of the spectra plotted in this section. The lower limit is due to the minimum frequency at which the (small) loudspeaker source is capable of emitting sufficient sound power, while the upper limit is f_{cut-on}. The EA is allocated on the other end of the duct, thanks to an appropriate parallelepiped casing where to clasp our EA. On the right of Fig. 20 there is the internal view of the tube.

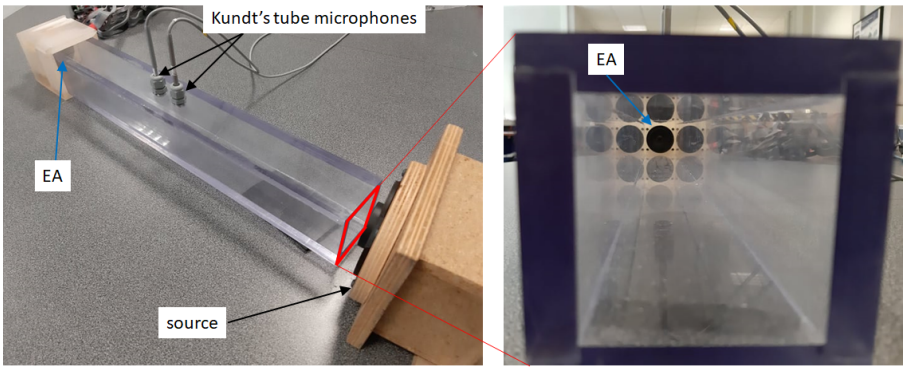

Figure 20. Kundt's tube.

4.1 Passivity tests

The absorption coefficient is retrieved according to the ASTM [44], to check the high-frequency behaviour induced by time delay and verify the contribution of each control parameter on the high-frequency passivity. Fig. 21 illustrates the variation of the absorption coefficient with the control parameters, as in the simulations of Fig. 4.

In the actual EA, the piston-mode modelled by Eq. (1) and taken into account in our control law (3), is only valid around the resonance frequency f_0 (which is about 500 Hz) of the uncontrolled EA. At about 1.5 kHz, another mode appears in Fig. 21, which anyway seems to be either amplified or weakened in a concordant way with the piston-mode. Nevertheless, an unexpected shortage of passivity appears at lower frequencies between 150 and 225 Hz, which is attenuated for higher values of μ_K and R_{at}. This effect is not due to the time delay but it might be related to dynamic uncertainties and spill-over effects [45] on a low-frequency mode of the speaker which is not taken into account in our control law, or to acoustic leakage inside the loudspeaker box. Another unwanted behaviour happens around the resonance frequency f_0 of the loudspeaker: the absorption coefficient presents a dip just before f_0, which critically descends toward the negative axis of α the more we shift the resonance frequency f_{at} of the EA with respect to f_0. This was predicted by the simulations of Fig. 4 but for higher values of μ_K/μ_M. The anticipation of the negative deep for lower values of μ_K/μ_M suggests either an underestimation of the time delay in simulations, or the presence of uncertainties in the Thiele-Small parameters. We remind that both dynamics and parameter uncertainties are the price to pay by a *model-inversion based* control, and their effects shall be investigated in a future contribution.

In this paper we focus on the time delay. Fig. 21 confirms that increasing μ_M raises the high-frequency absorption, reducing μ_K also slightly improves high-frequency passivity, while if R_{at} is significantly augmented an *excess of passivity* is promoted. These experimental trends are in agreement with the simulations of Section 3.1.

In Fig. 22 the absorption coefficient is measured for two different time delays. By reducing the number of microphones adopted by the EA (from four to two), it was possible to increase the sampling frequency f_s in the digital implementation, and consequently reduce the time delay which is directly linked to f_s. It is evident the improvement of high-frequency acoustical passivity obtained thanks to a shorter time delay. We also note that reducing the number of microphones adopted by the EA has no impact on the performance for normally incident plane waves, except for the low-frequency loss of passivity. This might be explained by an accentuation of the spill-over effect in using only two microphones instead of four, and probably suggests that the low-frequency mode of the loudspeaker (between 150 and 225 Hz) is asymmetric. In Fig. 23 the measured normal absorption of the EA, with $\mu_M = \mu_K = 0.3$ and $R_{at} = \rho_0 c_0$, is compared with the case of the layer of melamine foam applied in front of the speaker. The thicker the

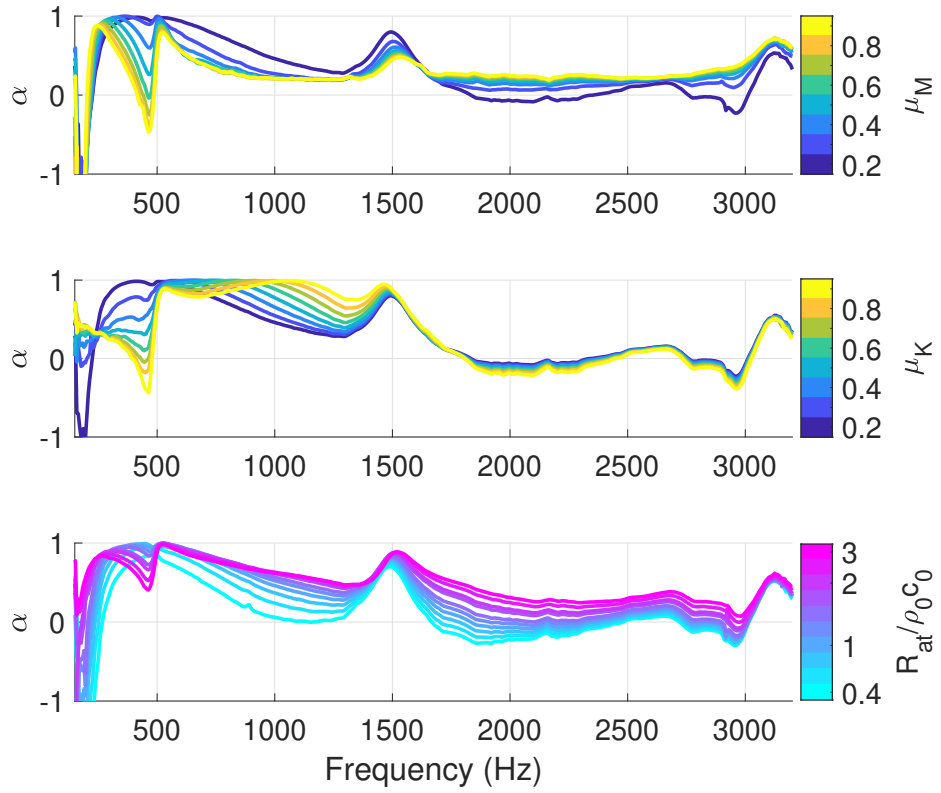

Figure 21. Variation of the measured normal absorption coefficient α with respect to the control parameters, in case of a delay in the control loop equal to $\tau = 2 \times 10^{-5}$ seconds. The default values chosen for the control parameters are $\mu_M = 0.2$, $\mu_K = 0.2$ and $R_{at} = \rho_0 c_0$.

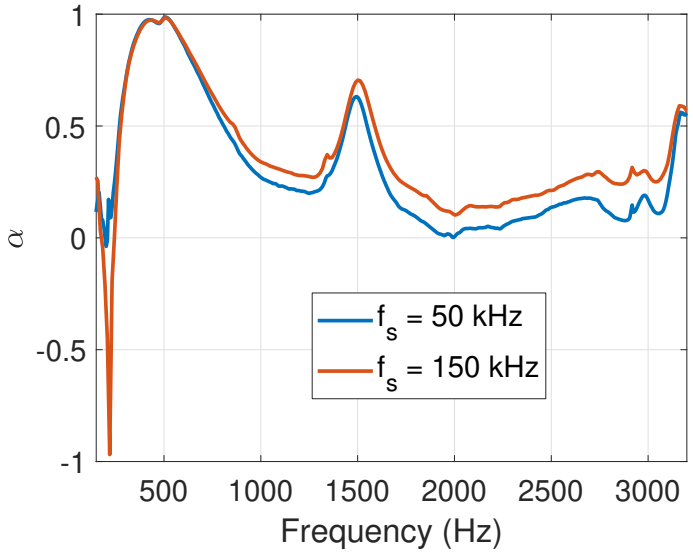

Figure 22. Measured normal absorption coefficient α for two different sampling frequencies f_s and consequent time delays. The control parameters are $\mu_M = 0.3$, $\mu_K = 0.3$ and $R_{at} = \rho_0 c_0$.

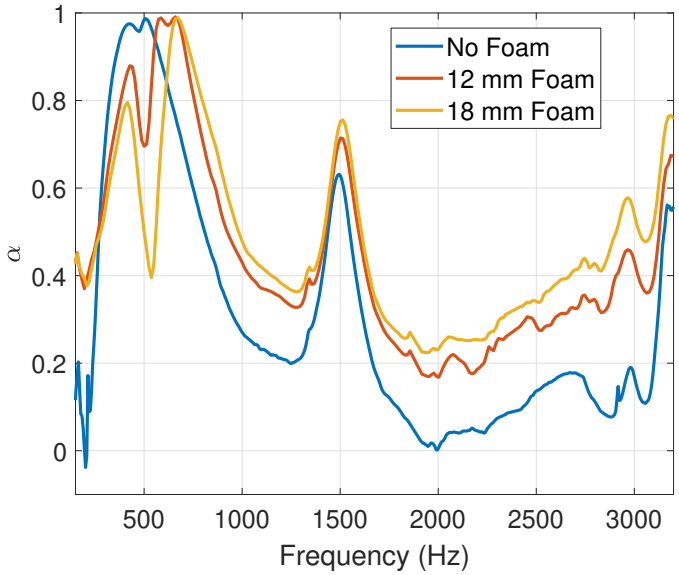

Figure 23. Measured normal absorption coefficient α in case of a layer of melamine foam applied of varying thickness.

porous layer, the more passivity is gained at high frequencies, whereas the EA performance at the resonance gets significantly modified. We can see that the addition of the foam layer increases the oscillation of α at f_0 (due to the non-coincidence of the pole and zero of $Y_a(s)$) induced by the time delay. Clearly, an additional dephasing is introduced, which is further increased if the foam does not fully cover the EA surface, but just the speaker. Fig. 17, in Section 3.4, proves that the non-uniform application of the foam adds-up to the oscillation of α at f_0. In Appendix C, also the effect of varying the flow resistivity σ is simulated according to the Miki semi-empirical model [40], in order to highlight how EA resonance is more affected for higher flow resistivities (as the porous becomes operative at lower frequencies), to the point of endangering acoustical passivity. In Fig. 17, we also note a slight shift toward higher frequencies of the resonance peak, which was not predicted by our simulations. Nevertheless, by modifying the porous model employed (Johnson-Champoux-Allard [39] instead of the Miki [40] one) along with proper porous properties identification, as well as taking into account the possibility of vibrational contributions of the foam, might allow to fully describe the actual impact of the porous. Section 3.4 and Appendix C provides useful avenues that should be accounted for to predict the resulting equivalent performances, as well as to successfully chose a proper passivating layer.

4.2 Stability tests

In this section we propose to experimentally assess the effect of the control parameters and the porous layer on the instability induced by time-delay. Presenting experimental results about the instability of a system, is not such a trivial task. Here, we use the time histories of sound pressure recorded in a hard-walled duct with the EA on one side and a rigid termination on the other, at the upsurge of instability. In Fig. 24 the experimental setup for the stability tests is shown. A Brüel and Kjaer impedance tube has been employed as hard-walled duct. The rigid termination is given by the rigid piston of the Brüel and Kjaer equipment. The EA is allocated on the right end side of the duct thanks to an appropriate cylindrical casing where to clasp our EA. The distance between the EA and the rigid termination is 0.24 m and the diameter of the duct is 0.1 m. In Fig. 25, the time history of the recorded sound pressure inside the cavity is plotted in case of EA with (red curve) and without (blue curve) the foam layer applied. The

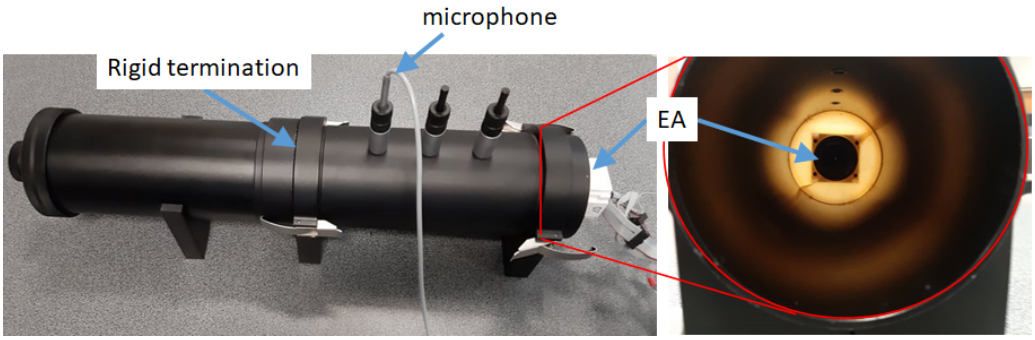

Figure 24. Experimental setup for stability tests. Brüel and Kjaer tube with rigid piston termination on the left and EA on the right.

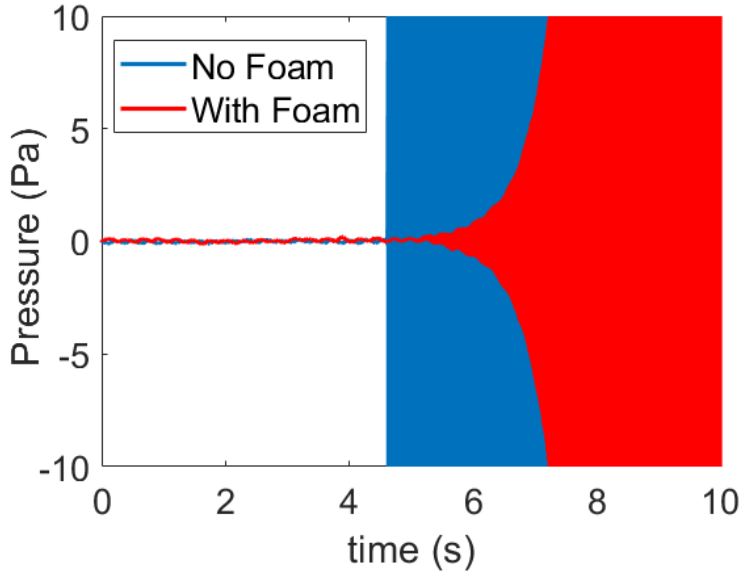

Figure 25. Time history of the pressure signal recorded at the upsurge of instability, in case of absence (blue curve) and presence (blue curve) of the 12 mm foam layer.

control parameters adopted are $\mu_M = \mu_K = 0.15$, $R_{at} = 3\rho_0 c_0$. As expected, with the porous layer the imaginary part of the unstable poles are lower (slower divergence of the time signal), i.e. the reflection coefficient is reduced (see Appendix A), as predicted by Fig. 16.
In Fig. 26, we recorded the time histories for different values of $\mu_M = \mu_K$ and of R_{at}, with the foam layer applied. The nominal values of the control parameters are: $\mu_M = \mu_K = 0.15$ for the R_{at} variation, and $R_{at} = \rho_0 c_0$ for the $\mu_M = \mu_K$ variation. We can see that augmenting $\mu_M = \mu_K$, as well as increasing R_{at} reduces the imaginary part of the unstable poles, as expected. For $\mu_M = \mu_K = 0.24$ and $R_{at} = \rho_0 c_0$, the system is stable.

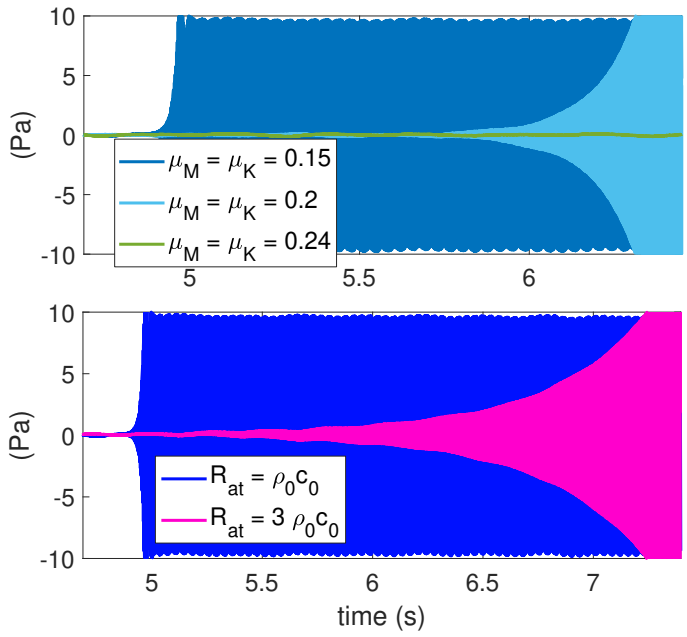

Figure 26. Time history of the pressure signal recorded at the upsurge of instability, for different values of $\mu_M = \mu_K$ and of R_{at}, with the foam layer applied.

5 Conclusions

The aim of this contribution was to increase the awareness about the main cause of instability, the time delay, in the application of a current-driven, pressure-based impedance control. The corrector is synthesized based upon model-inversion. First of all, we showed the effect of each target impedance parameter on the bandwidth of efficient absorption, and, in case of time delay, on acoustical passivity. Time delay affects the model-inversion at the original resonance of the actuator, endangering acoustical passivity around this frequency as more as the target resonance is shifted with respect to the original one. Such issue could be coped with, by properly designed compensators, based upon the precise identification of time delay. This will be addressed in the next contribution. More critically, time delay jeopardize high frequency acoustical passivity, which cannot be solved by classical compensators, because of an integral constraint which is for the first time presented and demonstrated in this paper. Therefore, we proposed a physical filtering of high-frequencies by a porous layer on the EA. Increasing the margin of acoustical passivity, the bandwidth of efficient absorption can be enlarged. Finally, we correlated the discussion on high-frequency acoustical passivity with instability upsurge, in case of a 1D cavity placed in front of the EA. The correlation has been conducted first analytically/numerically, and then experimentally.

Future work will be dedicated to synthesize correctors devoid of time-delay effects around the original resonance. For that purpose, time-delay should be identified precisely. The experimental tests in case of porous layer, demand deeper analyses on the interaction between the EA and the porous. An optimal design of the EA should take into account the acoustical passivity requirement since the very early stage design. This means to include the time-delay effects in the model-inversion, as well as to research optimal porous absorbers which would minimally affect the EA performance at the operative bandwidth, and maximally passivating it at higher frequencies. The inevitable impact of the porous passivation in the operative bandwidth should be compensated by re-defining the corrector in a slightly iterative process. Finally, as the integral constraint for purely passive systems allowed to design optimal absorbers with minimum thickness [30], analogously, our integral constraint presented in Section 3.2, might be exploited

for synthesizing optimal correctors with minimal energy supply. Such methods would be also enriched by more robust approaches, addressing both parameter and dynamic uncertainties.

Appendix A Instability in a 1D acoustic cavity

Let us consider a 1D hard-walled acoustic cavity as depicted in Fig. 27 with a rigid termination on one side and a generic acoustic element, which can consist of our EA, on the other.

According to the plane wave decomposition [46] the acoustic pressure in the duct is described by $p(x,t) = p^+(x,t) + p^-(x,t)$, where $p^+(x,t)$ and $p^-(x,t)$ are the forward and backward propagating plane waves respectively. Introducing the complex frequency $\Omega = \omega + \mathrm{j}\beta$ as in [46], the solution of the lossless wave equation can be written in terms of Fourier components, as:

$$\begin{aligned} p(x,t,j\Omega) &= p_0^+(\mathrm{j}\Omega)e^{\mathrm{j}(\Omega t - Kx)} + p_0^-(\mathrm{j}\Omega)e^{\mathrm{j}(\Omega t + Kx)} \\ &= p_0^-(\mathrm{j}\Omega)\Big(R(\mathrm{j}\Omega)e^{\mathrm{j}(\Omega t - Kx)} + e^{\mathrm{j}(\Omega t + Kx)}\Big), \end{aligned} \tag{17}$$

where $K = \Omega/c_0$ is the complex wave number and $R(j\Omega) = p_0^+(j\Omega)/p_0^-(j\Omega)$ is the complex reflection coefficient. By imposing the boundary condition on $x = 0$:

$$v(0,t,\mathrm{j}\Omega) = -Y_a(\mathrm{j}\Omega)p(0,t,\mathrm{j}\Omega), \tag{18}$$

where $Y_a(j\Omega)$ is the acoustic mobility at $x = 0$ (referred to the inward velocity, which explains the minus sign in Eq. (18)). For the Euler equation [46], the acoustic velocity is $v(x,t) = \frac{1}{\rho_0 c_0}p(x,t) = \frac{1}{\rho_0 c_0}(p^+(x,t) - p^-(x,t))$. Therefore, from Eq. (17) and (18), we retrieve the definition of the reflection coefficient [35]:

$$R(\mathrm{j}\Omega) = \frac{1 - Y_a(\mathrm{j}\Omega)\rho_0 c_0}{1 + Y_a(\mathrm{j}\Omega)\rho_0 c_0} \tag{19}$$

By imposing the rigid boundary condition on $x = L$:

$$v(L,t,\mathrm{j}\Omega) = p_0^-(j\Omega)\Big(R(\mathrm{j}\Omega)e^{\mathrm{j}(\Omega t - KL)} - e^{\mathrm{j}(\Omega t + KL)}\Big) = 0 \tag{20}$$

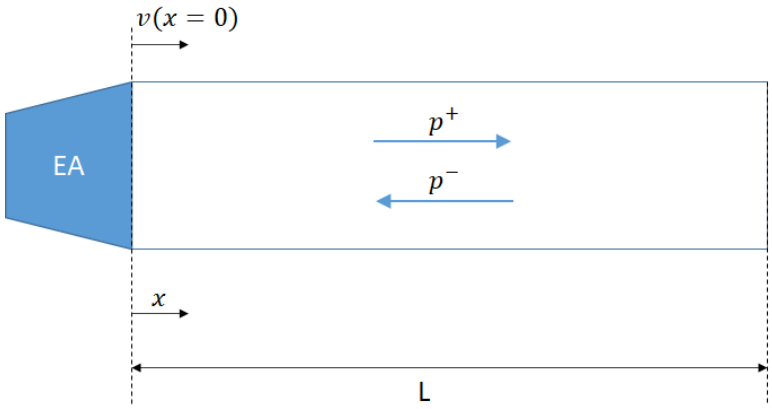

Figure 27. 1D hard-walled acoustic cavity with an EA on the left end and a rigid termination on the right end.

From Eq. (20), we get Eq. (21) and Eq. (22):

$$R(\mathrm{j}\Omega) = e^{2\mathrm{j}KL} = e^{2\mathrm{j}\omega/c_0 L} e^{-2\beta/c_0 L} \tag{21}$$

$$\ln|R(\mathrm{j}\Omega)| = -2\frac{\beta L}{c_0} \tag{22}$$

Therefore, a non-passive acoustical device (with $|R(j\Omega)| > 1$) in a lossless cavity, generates a negative value of β, which means instability. In Section 3.3 the analysis is carried out in terms of the Laplace variable s. The calculated poles s_p corresponds to $\mathrm{j}\Omega_p$, where Ω_p are the complex natural frequencies of the system. Therefore, an $|R(s_p)| > 1$ produces a $\mathrm{Re}\{s_p\} = -\beta > 0$. In addition, according to Eq. (21), the $\mathrm{Re}\{s_p\}$ increases in absolute value for shorter length of the duct, i.e. the upsurge of instability is quicker in a smaller acoustic cavity, as expected.

Appendix B The integral constraint on the reflection coefficient

Let us consider the complex function

$$\tilde{F}(s) = \frac{1}{s^2}\ln[\tilde{R}(s)], \tag{23}$$

where:

$$\tilde{R}(s) = R(s)\prod_n \frac{s + s_n^*}{s - s_n}. \tag{24}$$

By defining:

$$F(s) = \frac{1}{s^2}\ln[R(s)], \tag{25}$$

and:

$$G(s) = \frac{1}{s^2}\sum_n \ln\left(\frac{s + s_n^*}{s - s_n}\right), \tag{26}$$

then:

$$\tilde{F}(s) = F(s) + G(s), \tag{27}$$

The reflection coefficient transfer function $R(s)$ is multiplied by $\prod_n \frac{s+s_n^*}{s-s_n}$ in order for $\tilde{R}(s)$ to not have "unstable zeros" (zeros with positive real part). For a stable system then, $\tilde{R}(s)$ has neither poles nor zeros in the right-half complex plane (rhp) and $\ln[\tilde{R}(s)]$ is analytic in the rhp. The use of the natural logarithm in Eq. (23) is convenient in order to separate numerator and denominator of a rational function (like $R(s)$), which is indeed a common practice in deriving the Bode integral constraints in the classical control theory (see [32] for example). The s^2 at the denominator is present in order to compensate for the unboundedness of $\ln(\tilde{R}(s))$ for large $|s|$. Hence $\tilde{F}(s)$ is also analytic in the whole rhp except the origin, therefore for the Cauchy–Goursat Theorem [32]:

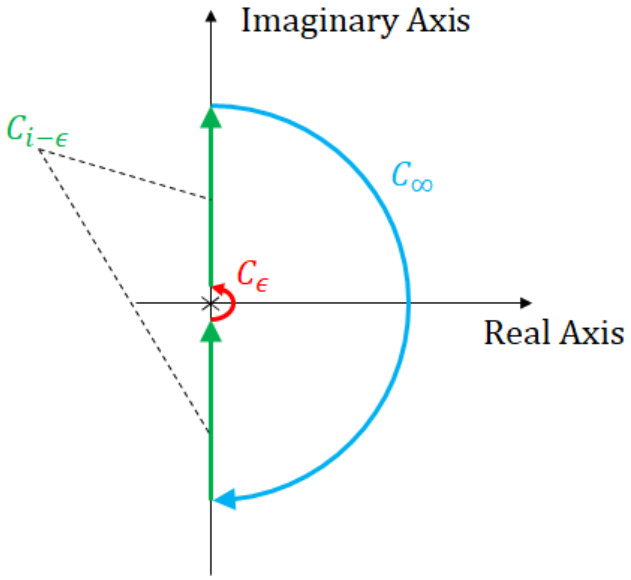

Figure 28. Contour in the complex plane for the application of the Cauchy Integral Theorem to the function $\tilde{F}(s)$ defined in Eq. (23).

$$\oint_C \tilde{F}(s)ds = 0 = \int_{C_{i-\epsilon}} \tilde{F}(s)ds + \int_{C_\epsilon} \tilde{F}(s)ds + \int_{C_\infty} \tilde{F}(s)ds. \tag{28}$$

where C_ϵ is the closed counter-clockwise right circular indentation at the origin, of infinitesimal radius ϵ, C_∞ is the clockwise semi-circle of radius which tends to infinity, and $C_{i-\epsilon}$ is the entire imaginary axis except the origin. Let us evaluate each integral on the rhs of Eq. (28). From the Residue Theorem [36]:

$$\int_{C_\epsilon} \tilde{F}(s)ds = \mathrm{j}\pi \mathrm{Res}\{F(s), 0\} + \mathrm{j}\pi \mathrm{Res}\{G(s)\}. \tag{29}$$

The residue of $F(s)$ in zero, $\mathrm{Res}(F(s), 0)$, is calculated reminding that $F(s)$ has a double pole in zero (the s^2 at the denominator).

$$\mathrm{Res}\{F(s), 0\} = \lim_{s\to 0} \frac{d}{ds} s^2 F(s) = \lim_{s\to 0} \frac{d}{ds} \ln(R(s)) = \lim_{s\to 0} \frac{d}{ds} \Big\{ \ln[1-\eta_a(s)] - \ln[1+\eta_a(s)] \Big\}. \tag{30}$$

The limit appearing in Eq. (30) can be separated in the two following contributions:

$$\lim_{s\to 0} \frac{d}{ds} \Big\{ \ln[1-\eta_a(s)] \Big\} = \lim_{s\to 0} \frac{-\frac{d\eta_a(s)}{ds}}{1-\eta_a(s)} = -\lim_{s\to 0} \frac{d}{ds}\eta_a(s). \tag{31}$$

$$\lim_{s\to 0} \frac{d}{ds} \Big\{ \ln[1+\eta_a(s)] \Big\} = \lim_{s\to 0} \frac{d}{ds}\eta_a(s). \tag{32}$$

where $\eta_a(s)$ is the normalized acoustic mobility of the controlled EA: $\eta_a(s) = Y_a(s)\rho_0 c_0$. Reminding the expression of $Y_a(s)$ of (7), it appears the mechanical mobility in the Open Circuit case $Y_{m0}(s) = 1/Z_{m0}(s)$ which has a zero in zero, and the controller $H(s)$ which must be a proper and stable transfer function. Hence, also $\eta_a(s)$ must have at least a zero in zero.
From the expression of $\eta_a(s)$ from Eq. (7), and developing the derivative, we find

$$\lim_{s\to 0} \frac{d}{ds}\eta_a(s) = \frac{\rho_0 c_0}{K_{a0}} \left(1 - \frac{Bl}{S_d} \lim_{s\to 0} H(s) \right). \tag{33}$$

Thus, from (30), (31) and (32), and (33), we get the integral along the first term on the rhs of Eq. (29):

$$\mathrm{j}\pi\mathrm{Res}\{F(s),0\} = -2\mathrm{j}\pi\frac{\rho_0 c_0}{K_{a0}}\left(1-\frac{Bl}{S_d}\lim_{s\to 0}H(s)\right). \tag{34}$$

The residual of $G(s)$ on the rhs of Eq. (29) instead sums up to zero, hence:

$$\int_{C_\epsilon}\tilde{F}(s)ds = -2\mathrm{j}\pi\frac{\rho_0 c_0}{K_{a0}}\left(1-\frac{Bl}{S_d}\lim_{s\to 0}H(s)\right). \tag{35}$$

Also the integral along C_∞, can be written in terms of the contribution of $F(s)$ and $G(s)$. From the Jordan's Lemma [36]:

$$\int_{C_\infty}\tilde{F}(s)ds = -\mathrm{j}\pi\lim_{s\to\infty}s\tilde{F}(s) = 0 \tag{36}$$

because

$$\lim_{s\to\infty}sF(s) = \lim_{s\to\infty}\frac{1}{s}\Big\{\ln[1-\eta_a(s)] - \ln[1+\eta_a(s)]\Big\} = -2\lim_{s\to\infty}\frac{1}{s}\eta_a(s) = 0. \tag{37}$$

and

$$\lim_{s\to\infty}sG(s) = \lim_{s\to\infty}\frac{1}{s}\left\{\ln\left(\frac{s+s_n^*}{s-s_n}\right)\right\} = 0, \tag{38}$$

Finally, since $F(s)$ is an even function of s according to its definition (25), the integral along $C_{i-\epsilon}$ becomes:

$$\int_{C_{i-\epsilon}}F(s)ds = \mathrm{j}\int_{-\infty}^{+\infty}F(\mathrm{j}\omega)d\omega = 2\mathrm{j}\int_0^{+\infty}F(\mathrm{j}\omega)d\omega \tag{39}$$

The contribution of $G(s)$ over $C_{i-\epsilon}$ is instead:

$$\int_{C_{i-\epsilon}}G(s)ds = -2j\pi\sum_n\frac{\mathrm{Re}\{s_n\}}{|s_n|^2}, \tag{40}$$

so we get the last contribution of $\tilde{F}(s)$ on $C_{i-\epsilon}$:

$$\int_{C_{i-\epsilon}}\tilde{F}(s)ds = 2\mathrm{j}\int_0^{+\infty}F(\mathrm{j}\omega)d\omega + 2j\pi\sum_n\frac{\mathrm{Re}\{s_n\}}{|s_n|^2} \tag{41}$$

Therefore, inserting Eq. (41), (36) and (34) in (28), we get the integral constraint:

$$-\int_0^\infty\frac{1}{\omega^2}\ln|R(\mathrm{j}\omega)|d\omega = \frac{\pi\rho_0 c_0}{K_{a0}}\left(1-\frac{Bl}{S_d}\lim_{s\to 0}H(s)\right) - \pi\sum_n\frac{\mathrm{Re}\{s_n\}}{|s_n|^2}, \tag{42}$$

We highlight that Eq. (8) is valid for any proper transfer function $H(s)$ applied as a controller in the current-driven, pressure-based impedance control. This means that for any type of controller $H(s)$ (even different from the one defined in Eq. 3 and analysed in this contribution), the integral constraint (8) still applies. We want to emphasize that such integral constraint, for purely passive resonators retrieves the one found by Yang in 2017 [30], which has its analogous for electro-magnetic waves in the work of Fano [47] and Rozanov [48]. The difference between our formalism (based upon the Laplace complex variable s, dearer to control engineers) and the one provided by [47], [48] and [30] (based upon the complex wave-length λ), is simply caused by

the fact that Eq. (8) presented in this paper, was originally obtained without awareness of the previous works of Fano, Rozanov and Yang.
Observe that this integral constraint is different from classical Bode's integral constraints on sensitivities (see [32]), as it does not apply to a sensitivity transfer function, but to a bilinear transform of the controlled system transfer function. Nevertheless, both Bode's integral constraints and the one provided in [30] (and extended here), are based on the *causality* condition.

Finally, we underline that the integral constraint on the reflection coefficient for normal incidence, remains valid for any angle of incidence as long as R_n is substituted by

$$R_\theta(\omega) = \frac{\zeta(\omega)/\sin\theta - 1}{\zeta(\omega)/\sin\theta + 1}, \tag{43}$$

where $\zeta(\omega)$ is the normalized acoustic impedance of the EA and θ is the angle of incidence, i.e. the angle between the incident pressure field and the tangent to the boundary (normal incidence is for $\theta = \pi/2$). For $\theta \neq \pi/2$ then, Eq. (8) still holds, with s_n being the zeros of $R_\theta(s)$.

Appendix C Equivalent impedance in case of porous layer applied just on the speaker

The experimental test-bench showed in Section 4 did not allow to fully cover the EA cell with the porous layer. Hence, only the speaker was layered by the melamine foam. This significantly affects the normal absorption. Below, we analytically derive the equivalent impedance assuming that the pressure used in the EA controller (p_m) is not filtered by the porous layer, see Fig. 29. Hence, the acoustic field cannot be considered as planar over the EA (on section 1). In order to find an analytically convenient expression, the hypothesis of plane wave has been retained: a plane wave field on the speaker is considered as different from the plane wave field on the microphone. Looking at Fig. 29, the acoustic variables are assumed as uniforms over the full section 2, while on section 1, the acoustic field is split in two parts: the one in front of the speaker (characterized by p_1, v_1), and the one in front of the microphone (defined by p_m). Assuming the plane wave between section 2 and the microphone position, we can write:

$$p_m = \cos(k_0 d) p_2 + \mathrm{j}\rho_0 c_0 \sin(k_0 d) v_2, \tag{44}$$

with $k_0 = \omega/c_0$. The p_m of Eq. (44) must be inserted in the loudspeaker dynamics Eq. (2). In turn, the acoustic variables on section 2, are obtained from the transmission matrix of Eq. (15), in terms of p_1, v_1. We can hence retrieve the effective acoustic mobility on the speaker diaphragm v_1/p_1:

$$Y_{a1} = Y_{a0} \frac{1 - \frac{Bl}{S_d} H e^{-\mathrm{j}\omega\tau} \left[\cos(k_0 d)\cos(k_c d) + \frac{\rho_0 c_0}{z_c} \sin(k_0 d)\sin(k_c d) \right]}{1 + Y_{a0} \frac{Bl}{S_d} H e^{-\mathrm{j}\omega\tau} \left[-\mathrm{j} z_c \cos(k_0 d)\sin(k_c d) + \mathrm{j}\rho_0 c_0 \sin(k_0 d)\cos(k_c d) \right]}, \tag{45}$$

By applying the translation theorem of Eq. (16), we can finally get the equivalent mobility on section 2. This simple analytical derivation serves to provide a fast estimation of the effect of placing the porous just in front of the speaker. In this simple analytical derivation, the plane wave assumption is a strong hypothesis, which neglects the actual non-planar effects. Nevertheless, it allows to quickly estimate the effect of placing the porous layer on the sole diaphragm, showed in Fig. 17.

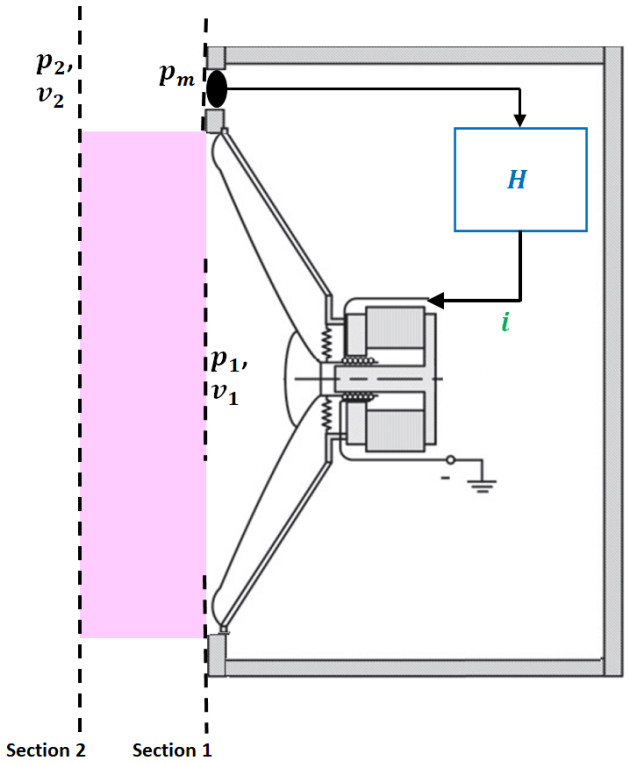

Figure 29. Sketch of EA with porous layer on speaker.

In order to give an indication about the impact porous properties have on the equivalent α, in Fig. 30 the flow resistivity σ has been varied in the Miki [40] semi-empirical model. In Fig. 30 the porous has been supposed applied on the entire EA, demonstrating the importance of the porous properties as well, on the equivalent absorption at resonance.

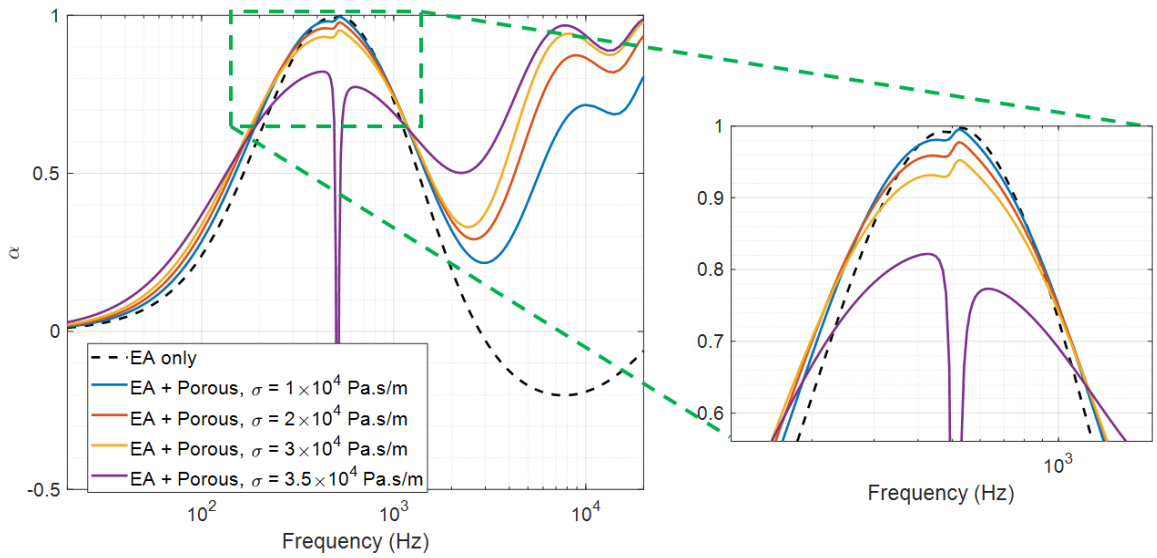

Figure 30. Effect of flow resistivity σ of a porous layer of thickness 12 mm, applied on the entire EA, on the absorption coefficient, with focus around resonance.

Acknowledgements

The authors acknowledge the support of the European Commission's Framework Program "Horizon 2020" through the Marie Sklodowska-Curie Innovative Training Networks (ITN) "SmartAnswer - Smart mitigation of flow-induced acoustic radiation and transmission" grant agreement No. 722401 to the present research project.

References

[1] G. E. Shambaugh, The Theory of Sound Perception, volume 1, Macmillan, 1930. doi:10.1121/1.1915184.

[2] D. Miljkovic, Active noise control: From analog to digital - Last 80 years, in: 2016 39th International Convention on Information and Communication Technology, Electronics and Microelectronics, MIPRO 2016 - Proceedings, IEEE, 2016, pp. 1151–1156. doi:10.1109/MIPRO.2016.7522313.

[3] D. Guicking, Patents on Active Control of Sound and Vibration: An Overview, D. Guicking, 2001.

[4] P. Lueg, Process of Silencing Sound, 1936.

[5] H. F. Olson, E. G. May, Electronic Sound Absorber, Journal of the Acoustical Society of America 25 (1953) 1130–1136.

[6] A. J. Fleming, D. Niederberger, S. O. Moheimani, M. Morari, Control of resonant acoustic sound fields by electrical shunting of a loudspeaker, IEEE Transactions on Control Systems Technology 15 (2007) 689–703.

[7] D. Guicking, E. Lorenz, An active sound absorber with porous plate, Journal of Vibration and Acoustics, Transactions of the ASME 106 (1984) 389–392.

[8] M.-A. Galland, B. Mazeaud, N. Sellen, Hybrid passive/active absorbers for flow ducts, Applied Acoustics 66 (2005) 691–708.

[9] L. Cremer, Theory regarding the attenuation of sound transmitted by air in a rectangular duct with an absorbing wall, and the maximum attenuation constant produced during this process, Acustica 3 (1953) 249.

[10] B. Tester, The optimization of modal sound attenuation in ducts, in the absence of mean flow, Journal of Sound and Vibration 27 (1973) 477–513.

[11] R. L. Clark, K. D. Frampton, D. G. Cole, Phase compensation for feedback control of enclosed sound fields, Journal of Sound and Vibration 195 (1996) 701–718.

[12] S. A. Lane, R. L. Clark, Active control of a reverberant enclosure using an approximate constant volume velocity source, in: Proceedings of the American Control Conference, volume 4, IEEE, 1998, pp. 2606–2610. URL: http://ieeexplore.ieee.org/document/703107/. doi:10.1109/ACC.1998.703107.

[13] J. Bao, P. L. Lee, B. E. Ydstie, Process Control: The Passive Systems Approach, IEEE Control Systems 30 (2010) 78–80.

[14] R. J. Bobber, An Active Transducer as a Characteristic Impedance of an Acoustic Transmission Line, The Journal of the Acoustical Society of America 48 (1970) 317–324.

[15] F. Orduna-Bustamantea, P. A. Nelson, An adaptive controller for the active absorption of sound, Journal of the Acoustical Society of America 91 (1992) 2740–2747.

[16] M. Furstoss, D. Thenail, M. Galland, Surface impedance control for sound absorption: direct and hybrid passive/active strategies, Journal of Sound and Vibration 203 (1997) 219–236.

[17] E. De Boer, Theory of motional feedback, IRE Transactions on Audio AU-9 (1961) 15–21.

[18] D. J. Leo, D. K. Limpert, Self-sensing technique for active acoustic attenuation, in: Collection of Technical Papers - AIAA/ASME/ASCE/AHS/ASC Structures, Structural Dynamics and Materials Conference, volume 4, American Institute of Aeronautics and Astronautics, Reston, Virigina, 1999, pp. 2603–2610. URL: http://arc.aiaa.org/doi/10.2514/6.1999-1530. doi:10.2514/6.1999-1530.

[19] T. Samejima, A state feedback electro-acoustic transducer for active control of acoustic impedance, The Journal of the Acoustical Society of America 113 (2003) 1483–1491.

[20] E. Rivet, S. Karkar, H. Lissek, Absorbeurs électroacoustiques pour l'égalisation modale des salles: une nouvelle approche avec des haut-parleurs à double bobine (Electroacoustic Absorbers for the modal equalization in rooms: a new approach with double coil loudspeakers), in: CFA Poitiers 2014, 2014, pp. 1157–1163.

[21] H. Lissek, R. Boulandet, R. Fleury, Electroacoustic absorbers: Bridging a gap between active sound absorption and shunt loudspeakers, 18th Int. Congr. Sound Vib. 2011, ICSV 2011 1 (2011) 141–148.

[22] R. Boulandet, H. Lissek, Toward broadband electroacoustic resonators through optimized feedback control strategies, Journal of Sound and Vibration 333 (2014) 4810–4825.

[23] E. Rivet, S. Karkar, H. Lissek, Broadband low-frequency electroacoustic absorbers through hybrid sensor-/shunt-based impedance control, IEEE Transactions on Control Systems Technology 25 (2016) 63–72.

[24] R. A. Pease, A Comprehensive Study of the Howland Current Pump A Comprehensive Study of the Howland Current Pump Applications for the Howland Current Pump AN-1515, Most 29 (2008) 12.

[25] E. T. J.-L. Rivet, Room Modal Equalisation with Electroacoustic Absorbers, Ph.D. thesis, EPFL, 2016. URL: https://infoscience.epfl.ch/record/222866. doi:10.5075/EPFL-THESIS-7166.

[26] R. Boulandet, H. Lissek, S. Karkar, M. Collet, G. Matten, M. Ouisse, M. Versaevel, Duct modes damping through an adjustable electroacoustic liner under grazing incidence, Journal of Sound and Vibration 426 (2018) 19–33.

[27] S. Karkar, E. De Bono, M. Collet, G. Matten, M. Ouisse, E. Rivet, Broadband Nonreciprocal Acoustic Propagation Using Programmable Boundary Conditions: From Analytical Modeling to Experimental Implementation, Physical Review Applied 12 (2019) 054033.

[28] X. Guo, H. Lissek, R. Fleury, Improving Sound Absorption Through Nonlinear Active Electroacoustic Resonators, Physical Review Applied 13 (2020) 014018.

[29] M. Xia, P. J. Antsaklis, V. Gupta, Passivity indices and passivation of systems with application to systems with input/output delay, in: Proceedings of the IEEE Conference on Decision and Control, volume 2015-Febru, IEEE, 2014, pp. 783–788. doi:10.1109/CDC.2014.7039477.

[30] M. Yang, S. Chen, C. Fu, P. Sheng, Optimal sound-absorbing structures, Materials Horizons 4 (2017) 673–680.

[31] L. L. Beranek, T. Mellow, Acoustics: Sound Fields and Transducers, Academic Press, Oxford OX5 1GB, UK, 2012. doi:10.1016/C2011-0-05897-0.

[32] G. C. Goodwin, S. F. Graebe, M. E. Salgado, Control System Design, volume 27, Prentice Hall New Jersey, 2007.

[33] S. Rienstra, Impedance models in time domain, including the extended Helmholtz resonator model, in: 12th AIAA/CEAS Aeroacoustics Conference (27th AIAA Aeroacoustics Conference), 2006, p. 2686.

[34] S.-I. Niculescu, K. Gu, Advances in time-delay systems, volume 38, Springer Science & Business Media, 2012.

[35] P. Filippi, A. Bergassoli, D. Habault, J. P. Lefebvre, Acoustics: basic physics, theory, and methods, Academic press, London NW1 7DX, UK, 1998.

[36] D. B. Scott, R. V. Churchill, J. W. Brown, Complex Variables and Applications, volume 69, Boston: McGraw-Hill Higher Education,, 1985. doi:10.2307/3617559.

[37] G. A. Baker, G. A. Baker Jr, G. A. BAKER JR, P. Graves-Morris, S. S. Baker, Padé approximants, volume 59, Cambridge University Press, Cambridge CB2 8RY, UK, 1996.

[38] A. G. Kelkar, S. M. Joshi, Robust control of non-passive systems via passification, in: Proceedings of the American Control Conference, volume 5, IEEE, 1997, pp. 2657–2661.

[39] J. F. Allard, N. Atalla, Propagation of Sound in Porous Media: Modelling Sound Absorbing Materials, John Wiley & Sons, 2009.

[40] Y. Miki, Acoustical properties of porous materials-Modifications of Delany-Bazley models-, Journal of the Acoustical Society of Japan (E) 11 (1990) 19–24.

[41] J. Steele, T. Green, Tame those versatile current source circuits, Electronic Design 61 (1992).

[42] K. Ugarte Agesta, Signal processing the human circulatory system for stability and regulation (2016).

[43] G. Matten, M. Ouisse, M. Collet, H. Lissek, S. Karkar, M. Versaevel, Synthèse temps-réel d'impédance acoustique distribuée, Technical Report, 2016.

[44] A. Standard, E1050-12,", Standard test method for impedance and absorption of acoustical materials using a tube, two microphones, and a digital frequency analysis system (2012).

[45] P. de Larminat, Automatique appliquée (Applied Automatic Control), Hermès Science publications/Lavoisier, Cachan, France, 2007.

[46] L. E. Kinsler, A. R. Frey, A. B. Coppens, J. V. Sanders, Fundamentals of acoustics, 1999.

[47] R. M. Fano, Theoretical limitations on the broadband matching of arbitrary impedances, Journal of the Franklin Institute 249 (1950) 57–83.

[48] K. N. Rozanov, Ultimate thickness to bandwidth ratio of radar absorbers, IEEE Transactions on Antennas and Propagation 48 (2000) 1230–1234.